

A theoretical unifying scheme for gamma-ray bright blazars

G. Ghisellini¹ \star , A. Celotti^{2,3}, G. Fossati², L. Maraschi¹ and A. Comastri⁴

¹ *Osservatorio Astronomico di Brera, via Bianchi 46, I-22055 Merate, Italy*

² *S.I.S.S.A., via Beirut 2-4, 34014 Trieste, Italy*

³ *Institute of Astronomy, Madingley Road, Cambridge CB3 0HA*

⁴ *Osservatorio Astronomico di Bologna, via Zamboni 33, I-40126, Bologna, Italy*

Received ***; in original form ***

ABSTRACT

The phenomenology of γ -ray bright blazars can be accounted for by a sequence in the source power and intensity of the diffuse radiation field surrounding the relativistic jet. Correspondingly, the equilibrium particle distribution peaks at different energies. This leads to a trend in the observed properties: an increase of the observed power corresponds to: 1) a decrease in the frequencies of the synchrotron and inverse Compton peaks; 2) an increase in the ratio of the powers of the high and low energy spectral components. Objects along this sequence would be observationally classified respectively as high frequency BL Lac objects, low frequency BL Lac objects, highly polarized quasars and lowly polarized quasars.

The proposed scheme is based on the correlations among the physical parameters derived in the present paper by applying to 51 γ -ray loud blazars two of the most accepted scenarios for the broad band emission of blazars, namely the synchrotron self-Compton and external Compton models, and explains the observational trends presented by Fossati et al. (1998) in a companion paper, dealing with the spectral energy distributions of all blazars. This gives us confidence that our scheme applies to all blazars as a class.

Key words: galaxies: active - quasars - BL Lacertae objects - jets - gamma-rays: theory - radiation mechanisms: non-thermal

1 INTRODUCTION

Among Active Galactic Nuclei (AGN) blazars represent the most extreme and powerful sources. The fundamental property characterizing blazars is their beamed continuum, due to plasma moving relativistically along the line of sight.

This scenario seems to apply to objects with somewhat different observational properties leading to different classifications/definitions. Objects with significant emission line equivalent widths are usually found as flat spectrum radio quasars (FSRQ). Objects without emission lines ($EW < 5 \text{ \AA}$) are classified as BL Lac objects. Different flavors of BL Lac objects have been found in radio and X-ray surveys. These also correspond to differences in the overall spectral energy distributions (SED) (see. e.g. Padovani & Giommi 1995), which have been interpreted either as due to orientation (Ghisellini & Maraschi 1989, Urry & Padovani 1995), or as intrinsic (Padovani & Giommi 1995). Nevertheless, while different sub-classes have different average properties, the actual distinction among them is certainly fuzzy and so far

several sources have shown intermediate behavior. In fact arguments for a substantial ‘continuity’ in the continuum spectral properties leading to adopt the blazar denomination as including both, BL Lacs as well as FSRQs, have been recently re-proposed by Maraschi et al. (1995), Sambruna et al. (1996) and Fossati et al. (1997).

The recent discoveries of about ~ 60 blazars emitting in the γ -ray band, by EGRET on board the Compton Gamma-Ray Observatory (CGRO) (Fichtel et al. 1994; von Montigny et al. 1995; Thompson et al. 1995; Mattox et al. 1997) and of a few BL Lac objects by WHIPPLE and HEGRA (Weekes et al. 1996, Petry et al. 1996), have revealed that the bulk of their radiative output is emitted in the γ -ray range, thus allowing us to discuss for the first time the characteristics of blazars knowing their total emission output and their entire SED. At the same time these observations have raised again the question as to whether and how the various subclasses differ in their γ -ray properties.

For a deeper understanding of the fundamental mechanisms at work in these sources it is crucial to address the questions: within the blazar phenomenon which is the physical origin of the difference among BL Lacs and even more

\star E-mail: gabriele@merate.mi.astro.it

broadly between BL Lacs and FSRQ? Is it possible to identify continuity among them, with a limited number of physical properties determining the observational characteristics of all blazars?

We address these issues from two sides: a purely observational approach (Fossati et al. 1998) based on complete sub-samples of blazars and (here) a more theoretical approach based on modeling individually the SEDs of all the γ -ray sources with sufficient available data to constrain their physical parameters. This allows us to derive trends between the physical quantities underlying the correlations between the observed ones.

Several models, still in competition, have been proposed to explain the γ -ray emission and the overall SED of blazars. Mannheim (1993) proposed that shock-accelerated electrons and protons give origin to two different populations of particles (electrons and electron-positron pairs), responsible of the entire SED through synchrotron emission. In an alternative widely adopted scenario, a single population of electrons is supposed to radiate from the far IR (or even radio) to the UV-soft X-rays by the synchrotron mechanism, and at higher frequencies by the inverse Compton process. In general the observed SEDs require curved spectra steepening at higher frequencies, for both the synchrotron and inverse Compton components. In the νF_ν representation of the SEDs each component shows then a peak that in the following will be referred to respectively as the synchrotron and inverse Compton peak. Specific models differ in the adopted geometry (one-zone homogeneous models or inhomogeneous jet models), and in the nature of the target photons which are up-scattered in energy by the inverse Compton process. The target photons could be either synchrotron photons (Maraschi, Ghisellini & Celotti 1992; Bloom & Marscher 1993; Ghisellini & Maraschi 1994), or be produced in the accretion disk (Dermer & Schlickeiser 1993), or in the broad line region (BLR). The BLR itself can be either illuminated by the disk (Sikora, Begelman & Rees 1994; Blandford 1993; Blandford & Levinson 1995), or self-illuminated by the jet (Ghisellini & Madau 1996). Finally, target photons could be produced by a dusty torus surrounding the blazar nucleus (Wagner et al. 1995). All these different scenarios have been tested on specific sources, but often more than one model can reproduce the same data with similar accuracy (see von Montigny et al. 1997 for 3C 273; Ghisellini, Maraschi & Dondi 1996 for 3C 279; Comastri et al. 1997 for 0836+710).

Here we examine only two of the leading pictures, namely the synchrotron self-Compton (SSC) and the ‘external Compton’ (EC) model, in which the main contribution to the target photons is produced outside the γ -ray emitting region, even if some contribution from the SSC component is always present. Therefore, in the following, with the term ‘EC’ we mean a model in which both the SSC and the EC contributions to the high energy spectrum are considered, while external photons are completely neglected in the SSC model. The SSC and the EC models are applied to all sources with sufficient available data to constrain the models themselves.

Through a search in the literature the multiwavelength overall spectra of 51 γ -loud blazars have been assembled. Even if the vast majority of the data are not simultaneous and the sample is not complete in any respect, they provide a useful template of the SED of different classes of γ -loud

blazars. While the non-simultaneity of the data (except for a few sources) precludes from deriving strong conclusions about specific objects, their large number allows us to study trends in the physical parameters of the models and possible correlations among them and with the observed spectral characteristics of different sub-classes of blazars.

In Section 2 the sample of sources is defined, while in Section 3 we describe the two adopted models, the computing procedures and the ‘fit’ criteria. The results are presented in Section 4 and discussed in Section 5.

2 THE SAMPLE

Two pieces of information have been considered essential for including a source in the present sample:

- (i) either detection and estimate of the γ -ray spectral slope in the EGRET band *or* detection by the WHIPPLE observatory;
- (ii) measured (or lower limit on) redshift.

For all the sources satisfying the above criteria sufficient information at lower frequencies could be found so that the location of both the synchrotron and inverse Compton peaks and the luminosity of each source could be estimated. The resulting 51 sources are listed in Table 1 in the Appendix, together with their redshift, classification and the list of references relative to the data plotted in Fig. 1a-f. The sample includes 14 BL Lac objects and 37 quasars. Among quasars, all core dominated radio sources with flat radio spectra, 16 are HPQ (highly polarized: optical polarization >3 per cent), 16 are LPQ (lowly polarized), while for the remaining 5, labeled NP, polarization measurements were not found.

BL Lacs can be divided in two sub-classes with different broad band spectra according to their radio-X-ray spectral index α_{RX} (Padovani & Giommi 1995, Fossati et al. 1998). In fact there is a close correlation between the value of α_{RX} and the energy of the synchrotron emission peak: for $\alpha_{RX} > 0.75$ this is in the IR-optical (LBL: low frequency BL Lac), otherwise in the UV-soft X-ray band (HBL: high frequency BL Lac). According to this definition, we have 10 LBL and 4 HBL.

Note that in our list there are two sources detected by WHIPPLE but not by EGRET, i.e. the two HBL objects Mkn 501 (1652+398) and 1ES 2344+514.

In Fig. 1a-f, the overall SEDs of all the blazars listed in Table 1 are plotted. Frequencies and luminosities are in the rest frame of the source and are calculated assuming cosmological parameters $H_0 = 50 \text{ km s}^{-1} \text{ Mpc}^{-1}$ and $q_0 = 0.5$. Fluxes have been dereddened using the absorption values reported in the NED database.

3 THE MODELS

3.1 General assumptions

The emitting region is assumed to be a sphere (blob) of constant radius R , with a homogeneous and tangled magnetic field B . Throughout the source relativistic electrons are continuously injected at a rate $Q(\gamma)$ [$\text{cm}^{-3} \text{ s}^{-1}$], corresponding to a luminosity L_{inj} and a compactness $\ell_{inj} \equiv L_{inj}\sigma_T/(Rm_e c^3)$, where σ_T is the Thomson scattering cross

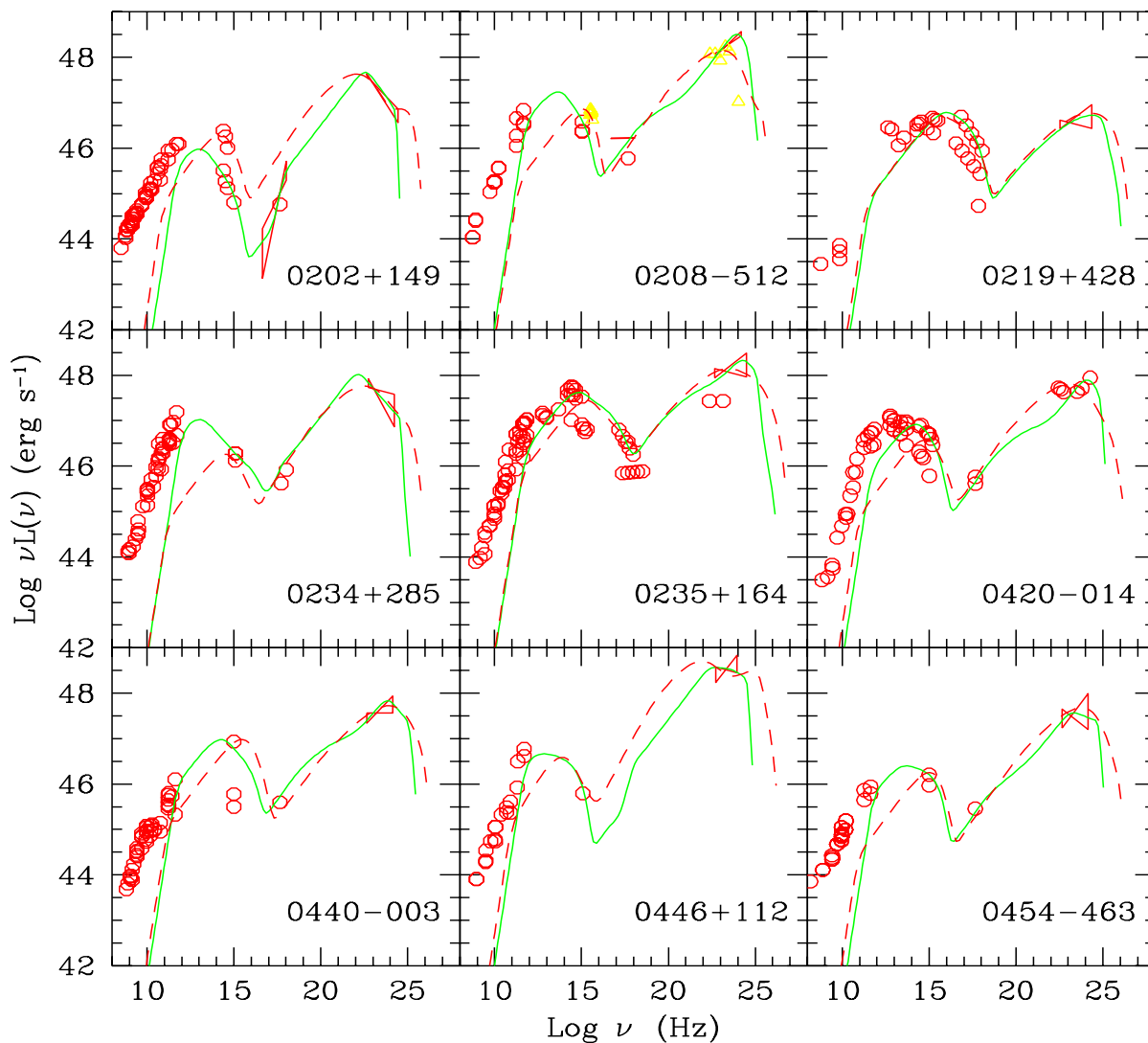


Figure 1. a. Spectral energy distributions (in $\nu L(\nu)$) of the 51 γ -ray loud sources. The broad band spectra have been assembled from data in the literature (the complete list of references is given in Table 1). In parenthesis the rescaling factors used for graphical purpose are indicated. SED from the SSC and EC models are superposed to the data, as dashed and solid line, respectively. The model parameters are reported in Table 2, in the Appendix. For 0716+714 a redshift $z = 0.3$ has been adopted.

section. This power is assumed to be entirely converted into radiation. The injected particles are distributed in energy as a power-law of slope s [$Q(\gamma) = Q_0 \gamma^{-s}$], between γ_{\min} and γ_{\max} .

The blob moves with a bulk velocity βc , corresponding to a Lorentz factor Γ , at an angle θ with respect to the line of sight. The Lorentz transformation of the specific intensity is thus given by $I(\nu) = \delta^3 I'(\nu/\delta)$, where $\delta = [\Gamma(1 - \beta \cos \theta)]^{-1}$ is the Doppler factor. For simplicity (see below), we always assume $\theta \sim 1/\Gamma$, resulting in $\delta \sim \Gamma$. In the following of this section, unless otherwise specified, all quantities are measured in the blob comoving frame.

We consider a stationary situation, that is we determine the particle equilibrium distribution and the spec-

trum of the emitted radiation self-consistently, assuming that the timescale over which the particles reach equilibrium is shorter than that over which the injection mechanism changes. We neglect particle escape and adiabatic expansion.

3.2 The particle distribution

The equilibrium particle distribution $N(\gamma)$ (cm^{-3}) is determined by the stationary solution of the continuity equation

$$N(\gamma) = \frac{\int_{\gamma}^{\gamma_{\max}} [Q(\gamma) + P(\gamma)] d\gamma}{\dot{\gamma}} \quad (1)$$

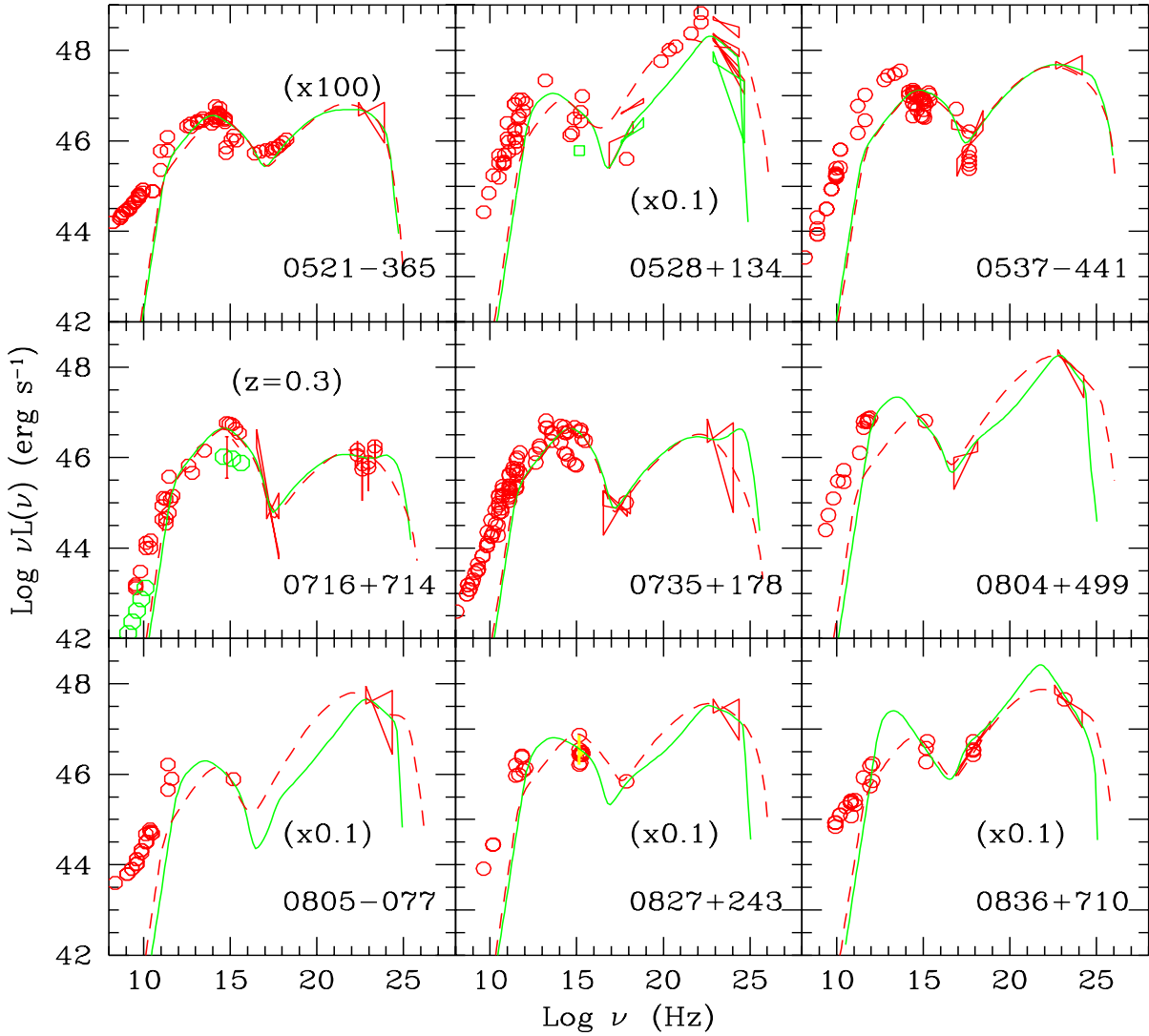


Figure 1. b Same as Fig. 1a

where $\dot{\gamma}$ is the cooling term and $P(\gamma)$ is the rate of electron-positron pair production. The only important mechanism for pair production is photon-photon collisions, the rate of which is calculated according to the prescriptions given in e.g. Ghisellini (1989).

$\dot{\gamma}$ takes into account the following cooling mechanisms:

(i) synchrotron emission: $m_e c^2 \dot{\gamma}_s = (4/3) \sigma_T c \gamma^2 U_B$, where $U_B = B^2/(8\pi)$ is the magnetic energy density;

(ii) inverse Compton emission: $m_e c^2 \dot{\gamma}_C = (4/3) \sigma_T c \gamma^2 U_r$, where U_r is the radiation energy density. Since the radiation spectrum extends to high energies, the scattering process has to be calculated by means of the Klein-Nishina cross section. For simplicity, we approximate it with a step function equal to the Thomson cross section for frequencies $x \equiv h\nu/(m_e c^2) \leq (3/4)/\gamma$, and zero otherwise. This implies that the radiation energy density effectively involved in the

inverse Compton cooling depends on the electron energy

$$U_r(\gamma) = m_e c^2 \int_0^{3/(4\gamma)} U(x) dx \quad (2)$$

The continuity equation is solved numerically, with an iterative approach, as described in Ghisellini (1989). The numerical treatment is necessary because of the high non-linearity of the processes involved: $N(\gamma)$ depends on the radiation spectrum (because of the inverse Compton cooling term and the pair production rate), which in turn is determined by $N(\gamma)$.

When the Klein-Nishina and pair production effects can be neglected, the solution of equation 1 is trivial: 1) for injection indices $s > 2$, we have a broken power law: $N(\gamma) \propto \gamma^{-2}$ up to γ_{\min} and $N(\gamma) \propto \gamma^{-s-1}$ above. In this case γ_{\min} can be identified with the crucial parameter γ_{peak} , i.e. the Lorentz factor of the electrons emitting at the peaks of

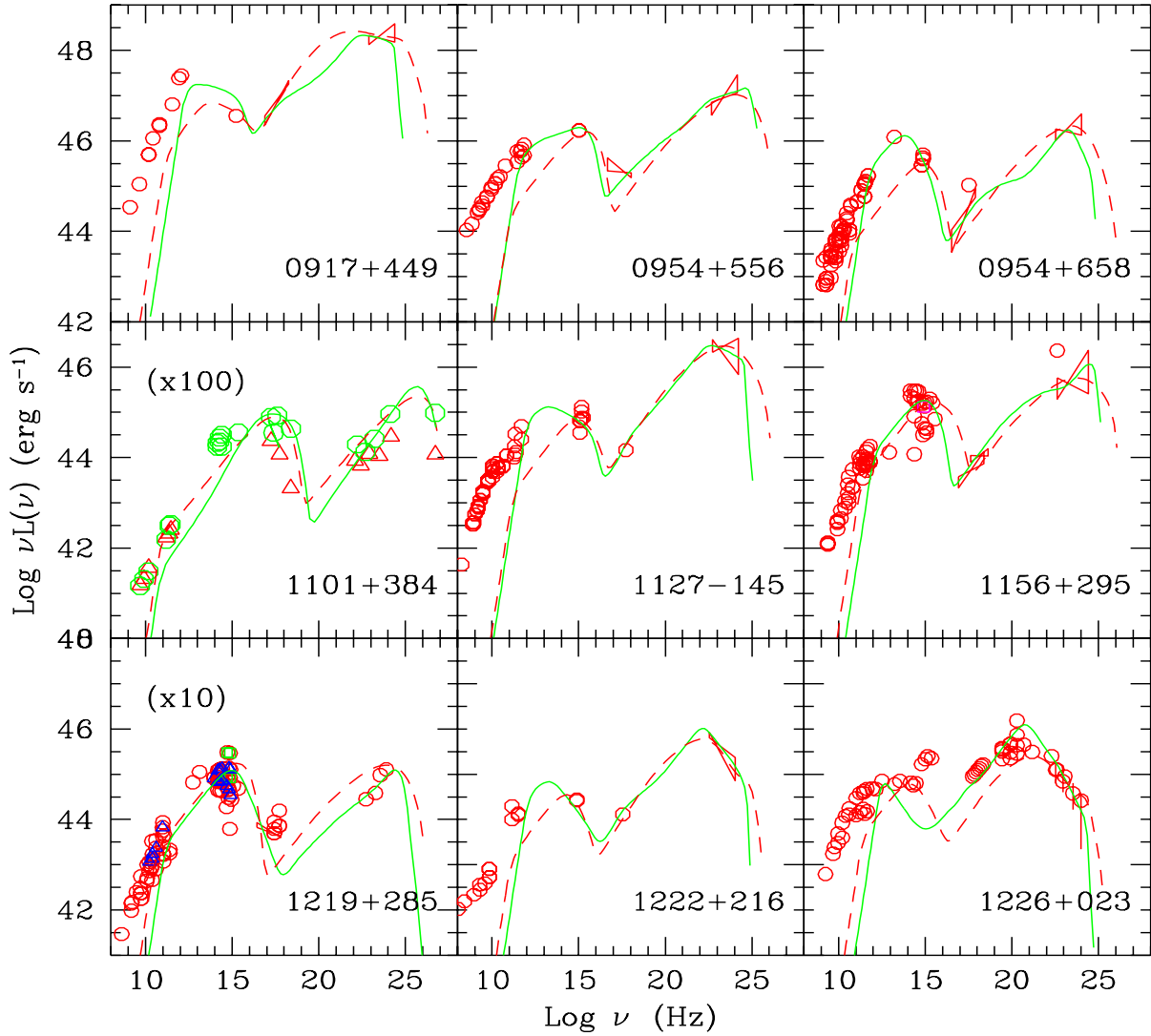


Figure 1. c Same as Fig. 1a

the synchrotron and inverse Compton components; 2) if $1 < s < 2$ we have the same solutions for $N(\gamma)$, but in this case $\gamma_{\min} < \gamma_{\text{peak}} < \gamma_{\max}$, since the spectral index of the radiation emitted by particles above γ_{\min} is flatter than unity; 3) if $s < 1$ the lower limit of the integral in equation 1 becomes unimportant, yielding $N(\gamma) \propto \gamma^{-2}$ in the entire energy range, except for γ close to γ_{\max} .

Note that the assumption of constant radius and no escape tends to overestimate the particle distribution at the lowest energies, where these effects are potentially more important than radiative cooling (if the overall compactness is much less than unity). This has no effect on the synchrotron spectrum, which is self-absorbed at low frequencies, and has no effect on the observable SSC spectrum, mainly made by high energy electrons. In the case of the EC model, instead, the X-ray spectrum is made by the sum of the EC and SSC components, and therefore the X-ray flux and spectrum can

depend on the details of the low energy particle distribution if the EC component dominates. Then in these cases the calculated X-ray spectrum could be flatter than what derived here.

3.3 Target photons

$U_r(\gamma)$ includes the contribution from the radiation both produced internally (by synchrotron and self-Compton emission) and externally to the blob.

The latter is assumed to be distributed as a (diluted) blackbody, peaking at a frequency $x_{\text{ext}} \equiv h\nu_{\text{ext}}/(m_e c^2)$ between 5×10^{-5} and 2×10^{-4} (in the rest frame of the blob). The exact value depends on the radiation mechanism responsible for the external field and the bulk Lorentz factor of the blob. The assumption of a blackbody spectral distribution is merely for ease of calculation. For instance, in the

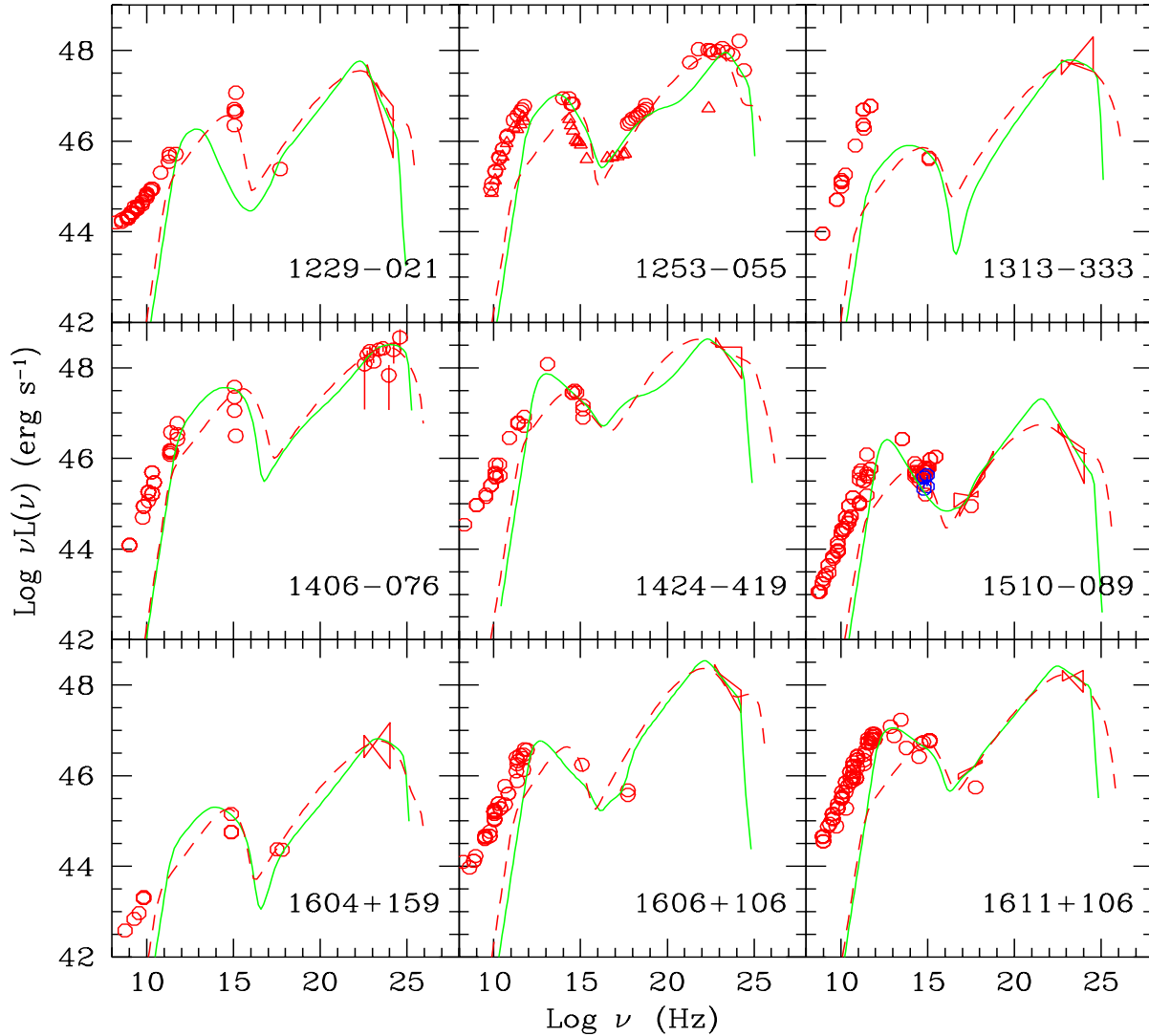


Figure 1. d Same as Fig. 1a

case of external radiation dominated by the broad emission line photons, an observer in the comoving frame of the blob would see a complex spectrum, not isotropic (blueshifted in the forward direction and redshifted in the opposite one): even a single, monochromatic line would be transformed into a peaked, but extended, spectrum.

Consequently, a peaked distribution can approximate the case of externally produced photons distributed in lines, independently of the origin of the photoionizing continuum: we can treat the cases of disk-illuminated as well as jet-illuminated BLR. On the other hand, this assumption can mimic the effect of an external scattering medium only if the illuminating continuum is narrowly distributed in frequency (e.g. radiation produced by an accretion disk), but it is not satisfactory for a scattering medium illuminated by the jet (which produces a more extended spectrum).

For a direct comparison with the value of the compact-

ness in injected electrons, ℓ_{inj} , we assume that also the external radiation can be characterized by an ‘effective compactness’ ℓ_{ext} , defined as

$$\ell_{\text{ext}} = \frac{\sigma_{\text{T}} R U_{\text{ext}}}{m_e c^2} \quad (3)$$

where U_{ext} is the radiation energy density (of the external radiation) as seen in the comoving frame, and is therefore amplified by a factor Γ^2 with respect to the same quantity measured in the frame of the observer.

As already mentioned, this external field is not isotropic in the comoving frame (see Dermer 1995). However both for simplicity and because of the uncertainty in the origin and therefore in the angular distribution of the external radiation, we assume an isotropic pattern for ℓ_{ext} (in the comoving frame). With this approximation also the inverse Compton radiation is isotropically distributed in this frame,

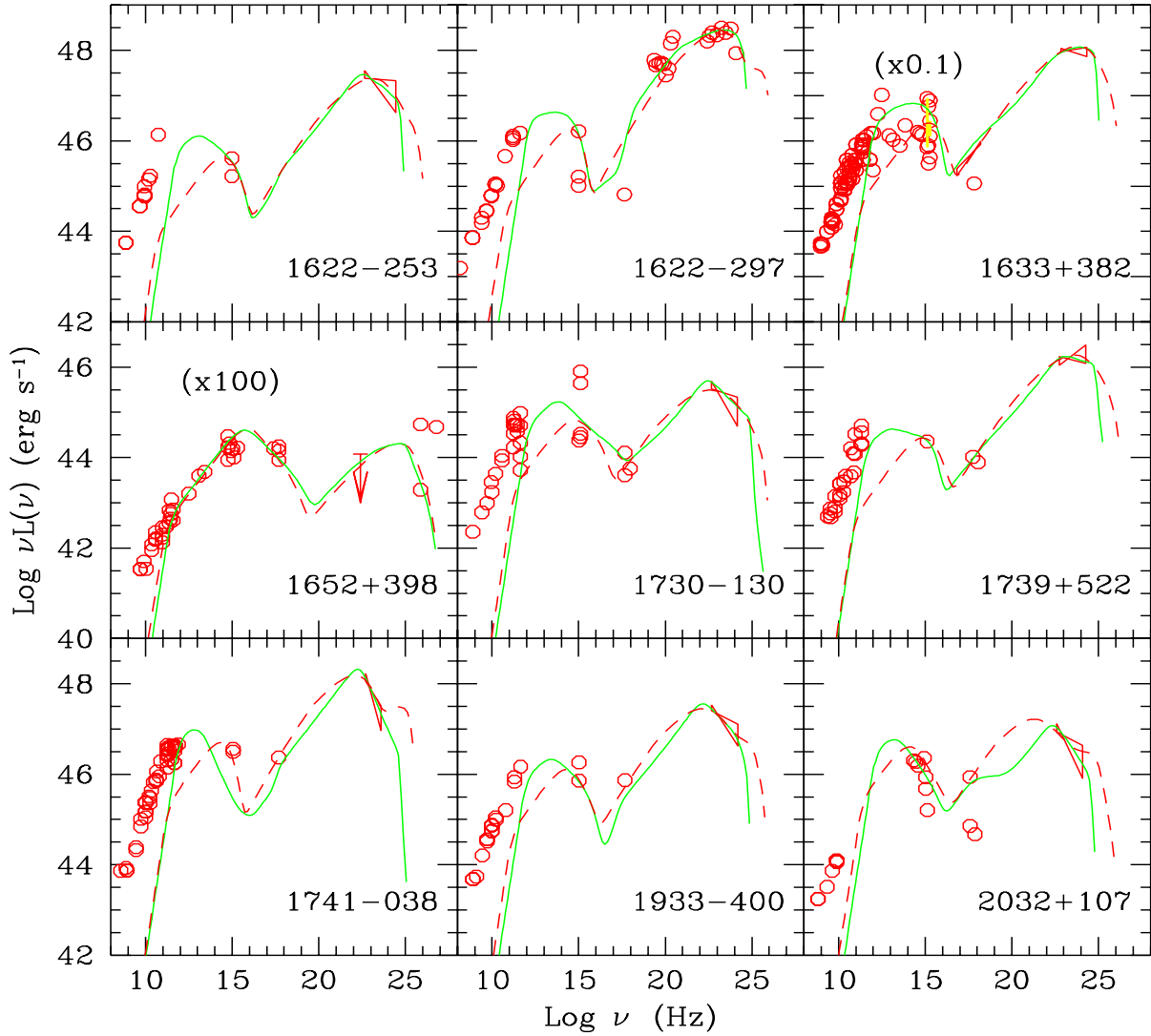


Figure 1. e Same as Fig. 1a

and subject to the same Lorentz transformation as the synchrotron and self-Compton emission.

The uncertainty related to the latter assumption can be estimated comparing the two extreme cases of the Compton flux emitted assuming (in the comoving frame) an isotropic seed photon distribution and the case of soft photons distributed only along the jet axis. Assume for simplicity that in both cases the seed photons are monochromatic, at the frequency ν'_0 . The total power emitted by an electron of energy $\gamma m_e c^2$ is $P = \sigma_T c U'_{\text{rad}} [\gamma^2 \int (1 - \beta \cos \phi)^2 d\Omega / (4\pi) - 1]$ (see e.g. Rybicky & Lightman 1979), where ϕ is the angle between the incoming photon and the electron velocity vector and U'_{rad} is the energy density of the seed photons. The viewing angle $\theta = 1/\Gamma$ corresponds to the aberrated angle $\theta' = 90^\circ$: at this angle, the power received in the isotropic case is $P_{\text{iso}} = (4/3)\sigma_T c U'_{\text{rad}}$, while the power received in the monodirectional case ($\phi = 90^\circ$) is

$P_{\text{mono}} = \sigma_T c U'_{\text{rad}} (\gamma^2/2 - 1)$. The ratio $P_{\text{mono}}/P_{\text{iso}}$ for large γ is therefore equal to $3/8$. The corresponding ratio between the scattered frequencies is equal to $3/2$.

3.4 Observational constraints

We require that the model parameters, besides giving a good description of the broad band SED, also satisfy additional constraints, regarding the observed variability timescales t_{var} and the amount of Doppler boosting. In fact, as commonly observed for the optical-UV and γ -ray emission of blazars, the minimum variability timescale must be as short as a day, or a fraction of a day. This corresponds to demand

$$R \lesssim c t_{\text{var}} \frac{\delta}{1+z} \quad (4)$$

with $t_{\text{var}} \sim 1$ day.

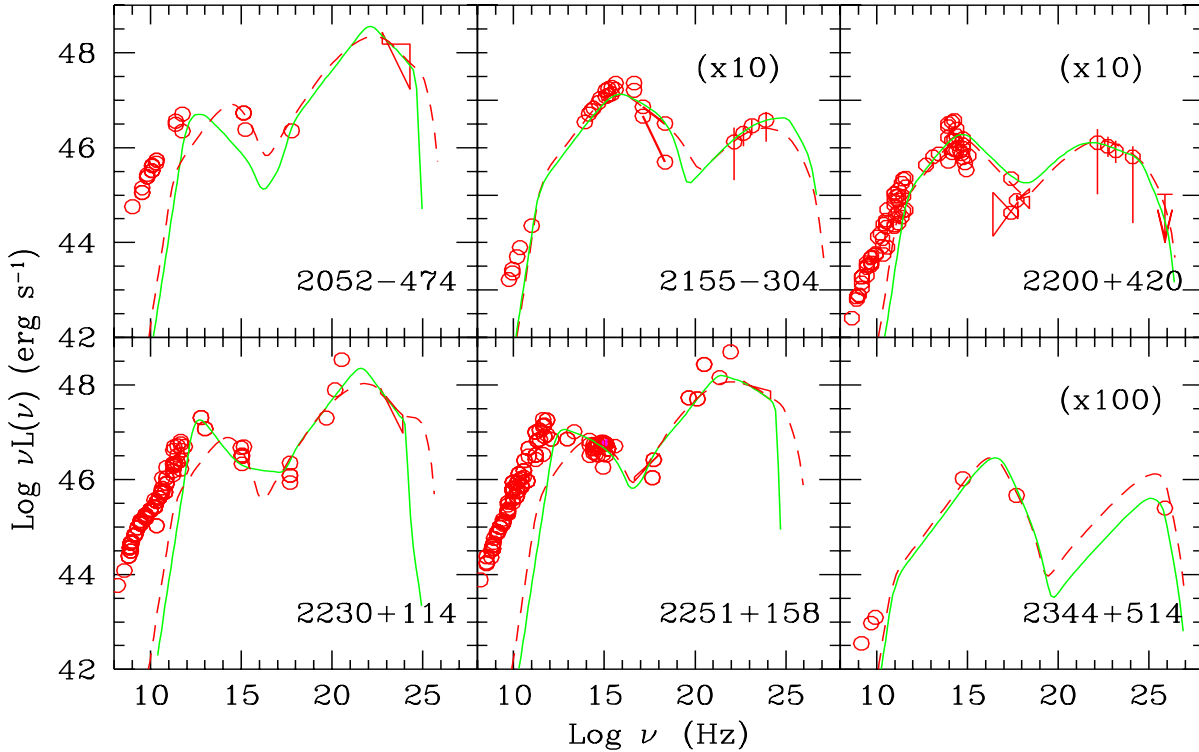


Figure 1. f Same as Fig. 1a

Furthermore, the Doppler factor is constrained not to exceed a value of 20–25, to be consistent with the observed superluminal speeds.

A third requirement, which is not imposed a priori but has to be satisfied in all cases, concerns the amount of pair production. As discussed in Ghisellini & Madau (1996), the γ -ray emitting region *must* be thin to the high energy radiation, otherwise it inevitably leads to overproduction of X-rays. The line of the argument is as follows: if a substantial fraction of the power emitted in the γ -ray band gets absorbed in photon–photon collisions, the pairs created (which are relativistic) radiate their energy in other bands by synchrotron and inverse Compton emission. In particular this results in a copious production of X-rays, with a luminosity of the same order as that in γ -rays. Since the importance of the pair production process is measured by the compactness, the transparency requirement translates into an upper limit to the allowed values of $\ell_{\text{inj}} \lesssim 1$ (see Dondi & Ghisellini 1995).

Summarizing, for the pure SSC model 7 input parameters are required, namely: R , B , Γ , ℓ_{inj} , s , γ_{min} , γ_{max} . If the inverse Compton scattering on external photons (EC model) is included, two more parameters are required ℓ_{ext} and x_{ext} (i.e. a total of 9).

However, if the slope of the injected electron distribution is steep ($s > 2$), which is the case for most sources, the exact value of γ_{max} becomes energetically unimportant and is practically irrelevant in the comparison with spectral data. Furthermore, if the external radiation is constituted

of broad line photons, the value of x_{ext} is constrained in a very narrow energy range.

In conclusion, even if there are formally nine free input parameters, γ_{max} is relatively unimportant, x_{ext} is tightly limited and constraints apply to the possible values of R , δ and ℓ_{inj} .

Given the number of free parameters, a key question concerns the uniqueness of the ‘fits’.

From an observational point of view, we have already mentioned the most critical quantities, namely the energy and luminosity of the two spectral peaks, which determine the global spectral shape. Furthermore, the optical-to-X-rays and the X-ray-to- γ -ray spectral indices and the three limits discussed above (on R , δ , ℓ_{inj}) also constrain the parameters.

In particular, as shown by Ghisellini et al. (1996), in the SSC scenario all the parameters are strongly constrained by the frequencies of the synchrotron and the self-Compton peaks, and by the corresponding powers. These allow to uniquely determine B , δ and ℓ_{inj} . R and ℓ_{inj} have then to satisfy the above constraints.

In the EC scenario, the further free parameter ℓ_{ext} could be in principle be constrained by the observed soft photon component (e.g. emission line intensities). Although we choose not to assume a priori the origin of the external soft photon field, however this should at least contain the contribution of photons produced in the broad line region. The addition of ℓ_{ext} as a free parameter makes the choice of δ not unique.

Independently of our assumption of selecting values of δ

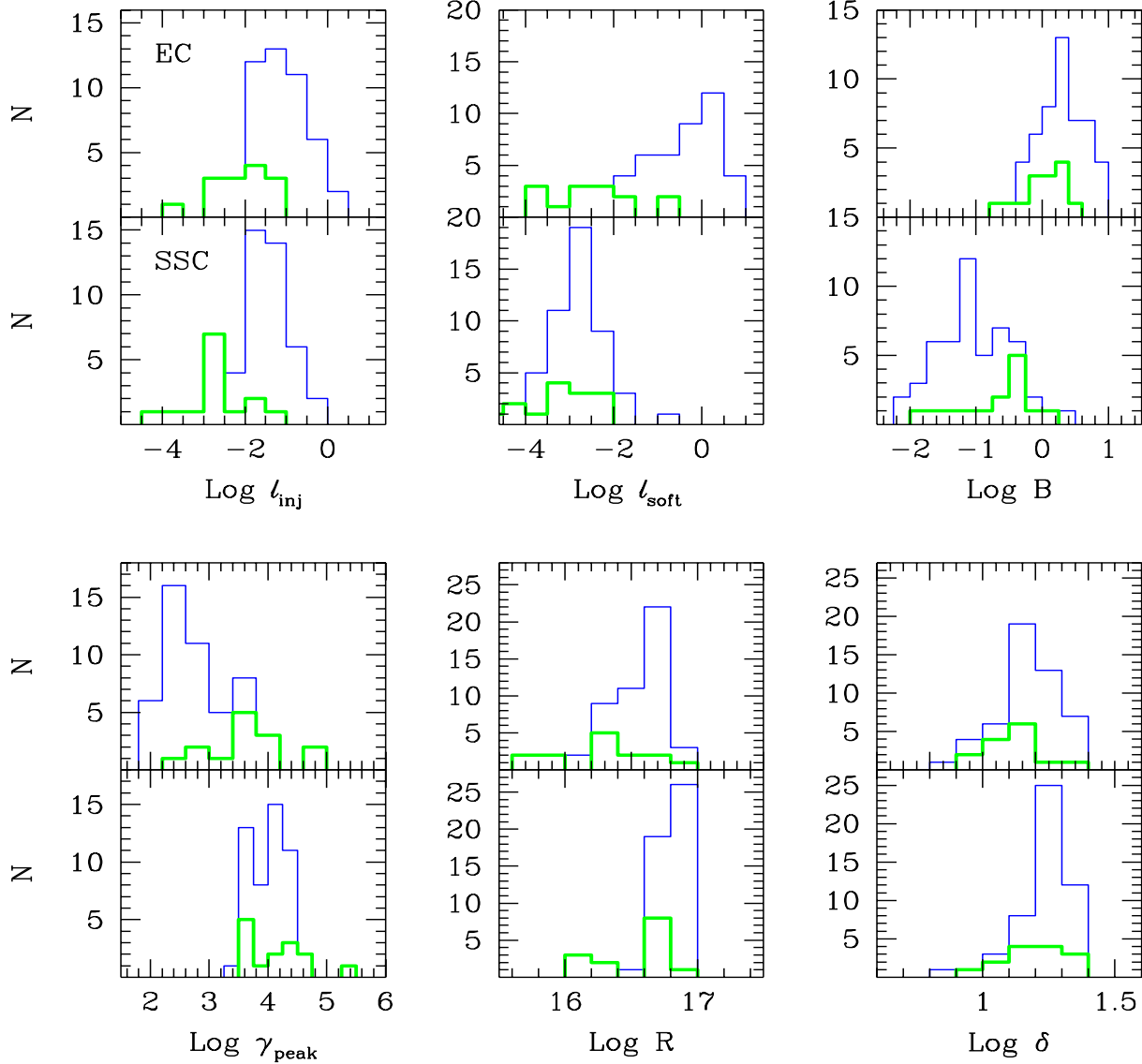


Figure 2. The histograms show the distributions of the parameters of the fits for the EC (upper panels) and the SSC (lower panels) models for all sources. Thick lines represent BL Lac objects. l_{soft} is l_{ext} in the case of the EC model and l_{syn} (compactness of the synchrotron radiation) in the case of the SSC model

consistent with the observed superluminal speeds, we have therefore examined the consequences of allowing arbitrary values of δ . In principle, one can obtain good fits with, e.g., $\delta \sim 100$ and small values of $l_{\text{inj}} (\propto \delta^{-4})$. But since $l_{\text{ext}} \propto \Gamma^2 \sim \delta^2$, the external photons become important as targets in collisions with very high energy γ -rays, with the result of overproducing X-rays (see §3.4 and Ghisellini & Madau 1996). Assuming instead a small value of l_{ext} corresponds to limit the broad line radiation to an implausibly small contribution. We therefore conclude that also the EC model is well constrained.

The main source of uncertainty on the model parameters is given by the incomplete and poor spectral coverage of several sources, which does not allow to determine with accuracy the observational constraints, most critically

the peak of the synchrotron emission. Another source of uncertainty regards the presence of other spectral components. Our single-zone and homogeneous models cannot reproduce the spectrum at frequencies below the far IR, since at these frequencies the model spectrum is self-absorbed. Other emitting regions, of greater dimensions, are necessary to fit the radio band. If these also emit in the IR and optical bands, they could contribute to the synchrotron spectrum, possibly shifting its peak at a frequency different from the one corresponding to the γ -ray emitting region.

As far as the actual fitting procedure is concerned, it should be pointed out that we try to reproduce collections of data that rarely are simultaneous, for sources whose variability is a defining property. Note also that the spectral coverage differs widely from object to object. On one hand

this makes it difficult to determine a method to estimate the goodness of ‘fit’ other than the visual inspection (with all its limits). On the other hand, as mentioned in the introduction, the main goal of our study is not to model specific blazars, but to unveil possible trends using a large number of sources. In this sense, although the model parameters relative to a specific source are not ‘objectively’ found (as it would be for a best fit determined through a statistical χ^2 test) nevertheless they represent a reasonable description of the spectral properties of each of the blazar in the sample.

4 RESULTS

The spectral distributions derived from the SSC and EC models which better describe the SEDs are superposed to the data in Fig. 1a-f. On the basis of these ‘fits’ *both* models can be acceptable for basically all sources. As mentioned in the Introduction, the EC model includes the contribution of the SSC component, i.e. the inverse Compton flux is calculated assuming, as seed photon flux, the sum of the internal synchrotron photons and the externally produced photons. As a rule, the EC component is always dominating at the highest frequencies (γ -ray band), and often it also dominates in the X-ray band. Note however that in some sources, as 0208–512, 0420–014, 0440–003, 0735+178, 0954+658, 1156+295, 1253–055 and 2032+107, the X-ray band is mainly produced by the SSC component even in the EC model.

In Table 2 (in the Appendix) the input parameters for all the fits are reported. The most remarkable difference between the two sets of parameters (SSC vs EC) is the relatively smaller value of the magnetic field in the SSC model. This has to be expected, since in order to reproduce the large ratios of inverse Compton to synchrotron luminosities, the SSC model requires a small magnetic energy density, while this constraint is relaxed in the EC scenario.

Although at first sight it seems difficult to discriminate between the two models, at least for FSRQ the parameters derived in the SSC scenario argue in favour of the EC model. In fact, let us consider the typical quantities required by the SSC model: $\delta \sim 20$, $\ell_{\text{inj}} \sim 0.03$, $B \sim 0.05$ G, $R \sim 10^{17}$ cm. These imply a compactness in synchrotron radiation $\ell_{\text{syn}} \sim 3 \times 10^{-3}$. Consequently, inverse Compton scattering on broad line photons is unimportant if the external radiation energy density U_{ext} (as seen in the comoving frame) is less than the synchrotron one, i.e.:

$$L_{\text{BLR}} < \frac{m_e c^3 \ell_{\text{syn}}}{\sigma_T R \Gamma^2} R_{\text{BLR}}^2 \simeq 3 \times 10^{42} R_{\text{BLR},18}^2 \text{ erg s}^{-1}, \quad (5)$$

where the above typical parameters have been used and $R_{\text{BLR}} = 10^{18} R_{\text{BLR},18}$ cm. This limit on L_{BLR} is certainly not observationally satisfied in FSRQ (e.g. Celotti, Padovani & Ghisellini 1997). For BL Lacs the situation is ambiguous. While the absence of observable emission lines in most BL Lacs suggests that the SSC process can dominate on the EC one, (weak) broad emission lines have been occasionally observed in some LBL (e.g. BL Lac itself, Vermeulen et al. 1995, Sitko & Junkkarinen 1985; PKS 0537–441, Stickel, Fried & Kühr 1993), sometimes exceeding the above limit. And indeed in some cases the inclusion of an external radiation component yields a better broad band fit. Therefore

in the following the discussion is focused on the results of the EC scenario. or HBL the different parameters derived in the SSC and EC models can be considered an indication of the allowed range of values and, in particular, the external radiation (e.g emission line luminosity) required by the EC fit can be taken as an upper limit.

Fig. 2 shows the distributions of values of the model parameters within the EC (upper panels) and the SSC (lower panels) scenarios. The thick solid lines correspond to the results for BL Lacs. In the EC case, BL Lac objects almost always form the left tail of the distributions, being characterized by smaller compactness, magnetic field and slightly smaller degree of beaming. On the contrary, comparable dimensions R and greater value of γ_{peak} are required by the EC fits of BL Lacs with respect to FSRQ. In the SSC case the required γ_{peak} is limited in a narrow range, without a clear distinction between BL Lacs and FSRQ, while BL Lacs are characterized by a larger average value of the magnetic field.

As a consequence of the constraints imposed on the Doppler factor and the variability timescales, the distributions of δ and R span less than one order of magnitude each, with $R \sim 10^{16-17}$ cm \dagger . On the contrary the other (intrinsic) quantities are spread over much larger ranges of values, with the external photon compactness covering the wider interval of about 5 decades.

The injected particle energy distribution is highly different from source to sources (see Table 2), in shape, compactness and (rather low) maximum energy $\gamma_{\text{max}} m_e c^2$, thus not requiring a very finely tuned injection/acceleration mechanism.

4.1 Correlations

The main goal of this work is to determine trends and correlations among physical quantities which can shed light on the relationship among different sub-classes of blazars and ultimately on the processes at work in these objects.

We have found that the most interesting quantity to investigate links among adopted and derived model parameters is the Lorentz factor at the break of the electron distribution γ_{peak} , which determines the location of both the synchrotron and the Compton peaks, and therefore largely determines the shape of the SED. The other important parameters controlling the SED are the ratio of the Compton to synchrotron powers, i.e. the Compton dominance L_C/L_{syn} , the power (or the corresponding compactnesses) injected in the form of electrons (which in our model corresponds to the radiated power), and the power in the external photon component. The results of linear correlations involving these quantities are shown in Figs. 3 and 4 and their statistical significance is reported in Table 3 in the Appendix. For completeness, we list in Table 4 (in the same Appendix) also the results of the linear correlations in the case of the SSC model.

Let us consider the results of the correlations:

\dagger Note that given the high values of the Doppler factors derived from the fits, the assumption $\theta \sim 1/\Gamma$ is satisfied. The only exception is 0521–365, which only requires $\delta \sim 1.4$

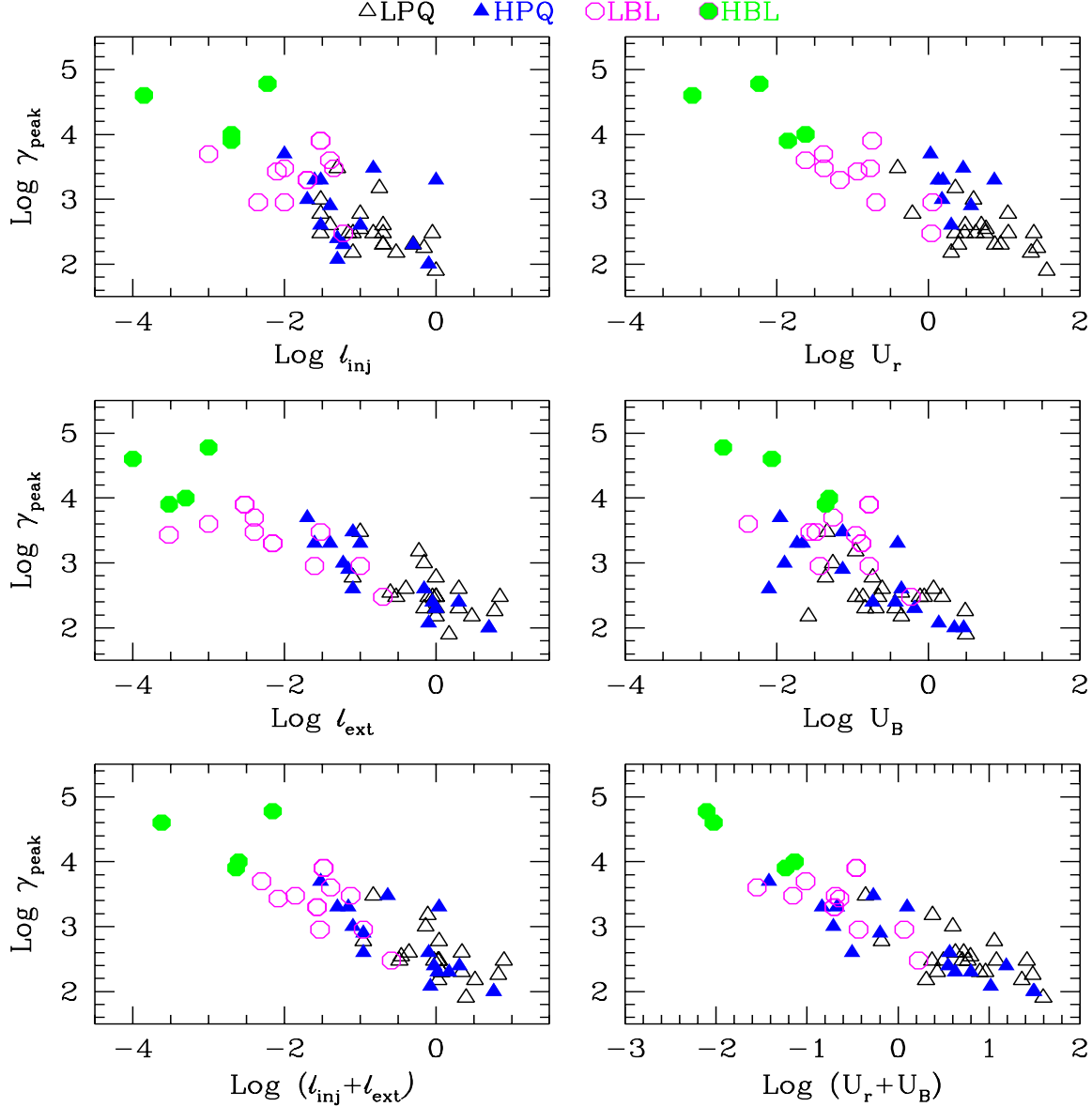


Figure 3. γ_{peak} (from the EC model) is plotted against some other, intrinsic, parameters. The statistical significance of the correlations is reported in Table 3, in the Appendix.

(i) γ_{peak} — Strong correlations are present between γ_{peak} and ℓ_{ext} , ℓ_{inj} and the energy densities in radiation U_r and magnetic field U_B , both for the whole sample and for the FSRQ sub-sample. In particular, a very strong linear correlation is found between γ_{peak} and the total energy density, with a dependence $\gamma_{\text{peak}} \propto (U_r + U_B)^{-0.6}$. The same trend appears from the correlation of γ_{peak} with $\ell_{\text{ext}} + \ell_{\text{inj}}$. It should be pointed out that these correlations are not, or at most only partly, induced by an observational selection effect: there would not be bias against detecting sources with either high values of γ_{peak} and $(U_r + U_B)$ or viceversa. Furthermore the significance of the correlations (i.e. their small spread) can be taken as a posteriori indication of the tightness of the observational constraints imposed on the model parameters. Note that HBL, LBL and quasars are located along a sequence.

(ii) L_C/L_{syn} — The Compton dominance correlates with γ_{peak} , ℓ_{ext} , ℓ_{inj} , and $\nu_{\text{peak}}^{\text{obs}}$, the latter being the *observed* peak frequency of the modeled synchrotron emission. It also correlates with the observed (beamed) power $L_{\text{inj}}^{\text{obs}} = L_{\text{inj}}\delta^4$, while only a weak correlation exists between L_C/L_{syn} and the magnetic field intensity. The statistical significance of all these correlations is higher when considering the entire blazar sample, while weakens when the subsamples of BL Lacs and FSRQ are considered separately. Again, note that in all cases BL Lacs are ‘separated’ from FSRQ, with HBL at the extremes and some LBL smoothly overlapping with FSRQ.

(iii) ℓ_{ext} vs ℓ_{inj} — A significant linear correlation is present when FSRQ are considered, while (most) BL Lacs show a relative deficiency in the external photon component with respect to this trend (see Fig. 5).

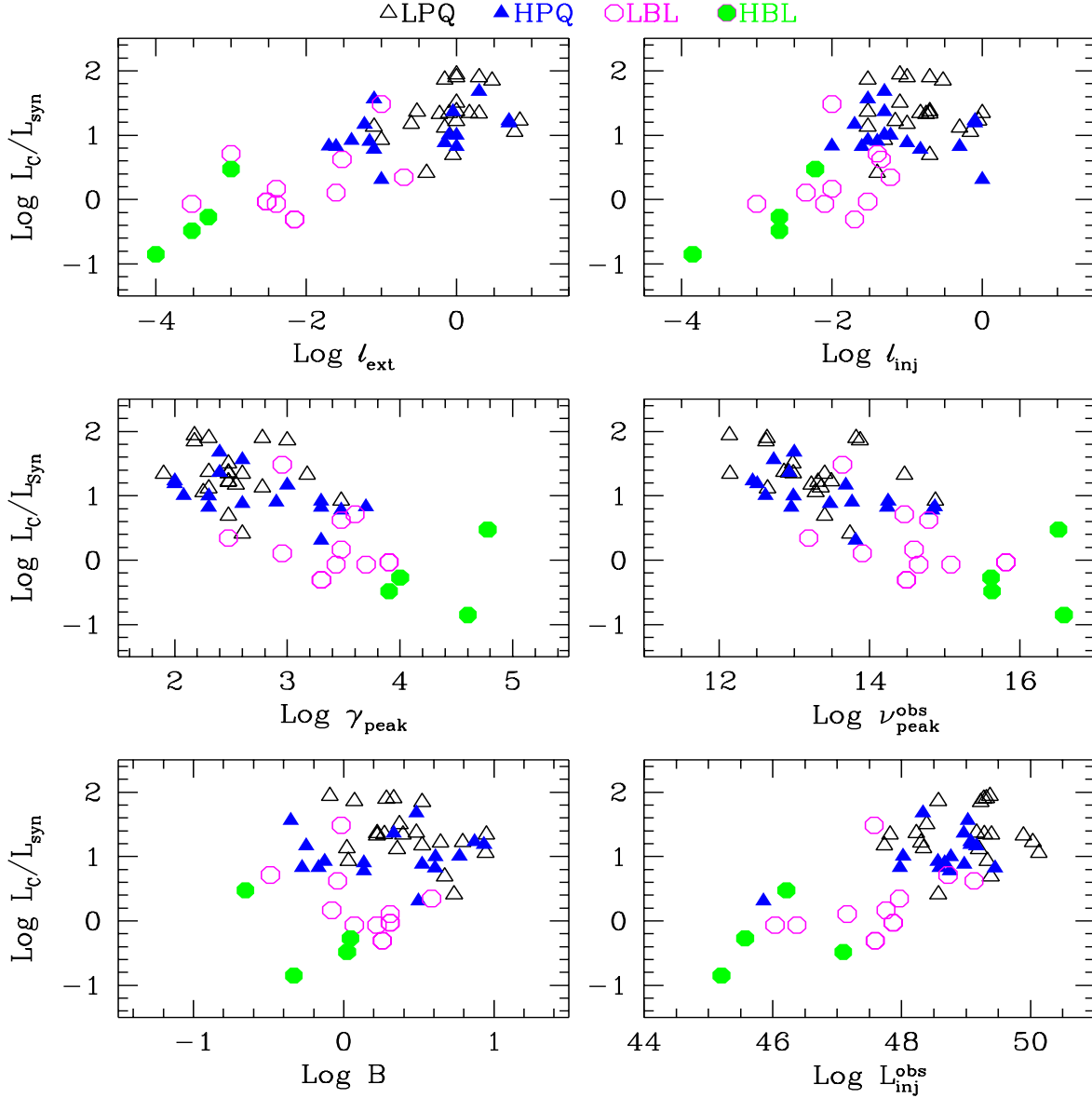


Figure 4. The Compton dominance L_C/L_{syn} as derived from the EC model is plotted against some other (both intrinsic and ‘observable’) parameters. The statistical significance of the correlations is given in Table 3.

To further investigate the correlations among the various quantities described above, we ran a principal component analysis (PCA) program on the correlation matrix. Briefly, the PCA is a method to describe a multidimensional ensemble of correlated parameters, by defining a new coordinate system in which each successive coordinate direction defined by the eigenvectors, explains as much of the remaining variance in the data as possible. PCA reduces the number of relevant components and the remaining should represent more basic parameters than the original ones. (see e.g. Boroson and Green 1992 for an application). We choose to present the PCA done with the 6 most important parameters of the fits: l_{inj} , l_{ext} , δ , γ_{peak} , B and R .

The results of the analysis are presented in Table 6 of the Appendix which lists the most significant eigenvectors in terms of their projection upon the original 6 quantities. At

the top of each column the percentage variance accounted for by the eigenvectors is given.

The first eigenvector accounts for about 45% of the total variance and is dominated by the contribution of the two compactnesses and the magnetic field energy density which anti-correlate (see above) with γ_{peak} . This eigenvector could be associated with the total power of the source. The largest contribution to the second eigenvector comes from δ , R and γ_{peak} , while the only relevant projection on the third one is due to γ_{peak} .

Given that the Doppler factor δ and the blob dimension R are not completely independent quantities (see section 3.4), the PCA analysis points to γ_{peak} , l_{inj} and l_{ext} as fundamental variables in explaining the formation of the blazar SED, and confirms the results found through the linear regression analysis.

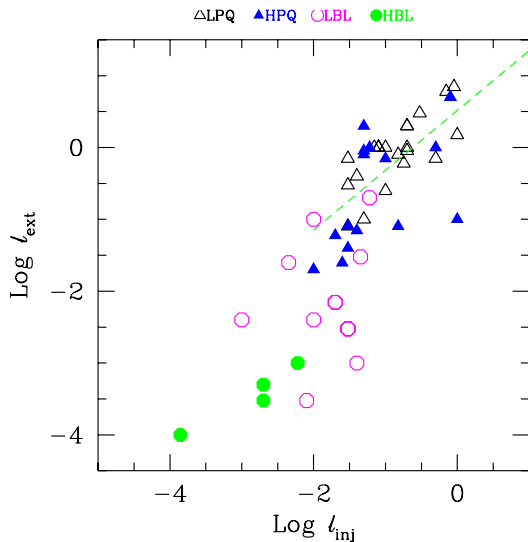


Figure 5. The relation between the compactnesses in external photons ℓ_{ext} and injected power ℓ_{inj} . The line represents the best-fit linear correlation for FSRQ only.

5 DISCUSSION AND CONCLUSIONS

5.1 Generalities

We examined and reproduced the broad band spectral properties of a sample of 51 γ -ray loud blazars, in terms of synchrotron and inverse Compton emission from a homogeneous (one-zone) model. This gives a reasonable good description of the observations at frequencies greater than typically $\sim 10^{11}$ Hz. The radio emission is expected to be produced by less compact regions on larger jet scales.

On the basis of the ‘fits’, it is difficult to determine whether the seed field for the inverse Compton scattering is mostly provided by synchrotron or external photons. However, as pointed out by Sikora et al. (1994), the presence of broad emission lines, together with the found values of δ , make photons produced externally to the emitting jet unavoidably important. For this reason we consider the parameters derived in the EC scenario as the most likely for all quasars and some BL Lacs.

Strong correlations have been found among the physical parameters derived from the EC model.

Of particular physical interest is the strong correlation between the energy of electrons emitting at the peak of the observed spectra and the total energy density present in the emitting region, $\gamma_{\text{peak}} \propto (U_r + U_B)^{-0.6}$. One way to explain this is to assume that γ_{peak} is the result of a competition between the radiative cooling and the (re-)acceleration process, i.e. $\dot{\gamma}_{\text{acc}}(\gamma_{\text{peak}}) \sim \dot{\gamma}_{\text{cool}}(\gamma_{\text{peak}})$. The typical emitting electron would in this case be quickly accelerated up to the energy where cooling is important, while only a few particles would be accelerated at higher energies. The found correlation would then imply that the (re-)acceleration process is almost independent of both the energy density in the region (both in radiation and in magnetic field) and the energy of the particles, since $\dot{\gamma}_{\text{cool}}(\gamma_{\text{peak}}) \propto \gamma_{\text{peak}}^2 (U_r + U_B) \sim \text{const.}$ In addition, the injected particle distribution does not require characteristic shape and/or maximum energy. We postpone

the discussion of this interesting result to future work; here we would only like to mention the ‘hot jet’ model put forward by Sikora et al. (1997), in which the balance between heating and cooling can lead to a formation of a peak in the electron energy distribution.

We found another strong correlation between γ_{peak} and the Compton dominance L_C/L_{syn} . On one side this simply confirms and quantifies, from a different perspective, the observational trends pointed out by e.g. Fossati et al. (1998) on the relation between the dominance of the Compton/ γ -ray emission and the energy of the peaks of the two spectral components for complete samples of blazars. On the other side, it suggests that this link can be simply interpreted as the consequence of a change in the radiation energy density of the external field. An increase in the latter in fact leads to an increase in the particle Compton cooling and therefore both to a decrease in γ_{peak} and a relative increase in the γ -ray luminosity. Once again we stress, as discussed in the next Section, that different sub-classes of blazars are located in different areas of this correlation.

As expected from the above correlations γ_{peak} is also (inversely) related to the power injected in the form of relativistic emitting particles.

As presented in Fossati et al. (1998), the ratio of the frequency of the Compton (ν_C) to the synchrotron (ν_{syn}) peak is compatible with being approximately constant. Our results are in agreement with these findings, despite the relatively wide range spanned by γ_{peak} (~ 3 decades for the EC model). In fact in the EC scenario (and in the Thomson regime of the inverse Compton process), $\nu_C/\nu_{\text{syn}} \sim \Gamma\nu_{\text{ext}}/\nu_B$, is independent of γ_{peak} (here $\nu_B = eB/(2\pi m_e c)$ is the cyclotron frequency), and the narrow range of values of B found in the EC model can account for the approximate constant ratio of ν_C/ν_{syn} .

In the SSC model, instead, it is γ_{peak} which is found in a narrow range (less than 2 decades). In the SSC case, we expect $\nu_C/\nu_{\text{syn}} \sim \gamma_{\text{peak}}^2$ (in the Thomson regime), and $\nu_C/\nu_{\text{syn}} \sim \gamma_{\text{peak}}^{-1}$ in the extreme Klein-Nishina regime (in this case $h\nu_C \sim \gamma_{\text{peak}} m_e c^2$).

5.2 The blazar unification

Evidence for continuity in the observed spectral properties of BL Lacs and FSRQ have been recently found by Fossati et al. (1998), by studying complete samples of sub-classes of blazars in different energy bands. Diagrams and quantities derived by Fossati et al. (1998) from either data or their analytical representation turn out to be similar to and consistent with those found in this paper through model fitting. In Fig. 6, the model considered here is applied to the average SEDs derived by Fossati et al. (1998) by binning, according to the radio luminosity, both BL Lacs and FSRQ belonging to complete samples. The parameters of these fits are reported in Table 5 in the Appendix. The fact that the model fits the average SEDs derived from complete blazar samples, with similar parameters and trends as for the γ -ray blazars, gives us confidence that our results are valid for all blazars.

The main result of the present paper concerns the intrinsic relationship among phenomenologically different classes of blazars, and in particular the evidence for a well

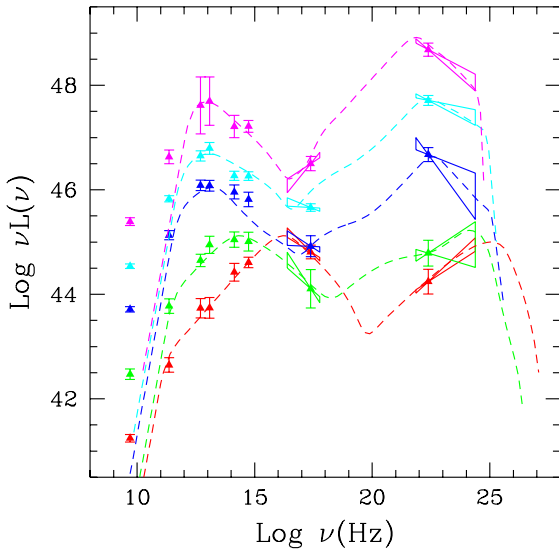


Figure 6. Fits with the EC model of the average SEDs derived by Fossati et al. (1998). BL Lacs and FSRQ belonging to complete samples have been divided in bins accordingly only to their radio luminosity, and the average fluxes in each bin have been computed. The model parameters are reported in Table 5 (Appendix), and are in complete agreement with the parameters determined for the γ -ray loud sources examined in this work.

defined sequence in the properties of HBL, LBL and FSRQ with increasing importance of an external radiation field: the observed spectral properties of HBL, LBL, HPQ and LPQ can be therefore accounted for by e.g. the increasing role of broad emission line radiation (see also Fig. 6 and Table 5). This in fact dictates the peak energy of the emitting particle distribution and hence the shape of the spectra, thus determining the classification of an object into one of the blazar flavors. The fundamental physical processes occurring in and outside the relativistic jet are instead the same. This is indicated by the correlation between ℓ_{ext} and ℓ_{inj} , which seems to ‘set in’ for more powerful object, from LBL up to the most luminous LPQ (see Fig. 5).

This proposed blazar unifying sequence can be therefore summarized as follows (see the schematic sketch in Fig. 7):

(i) HBL are sources characterized by the lowest intrinsic power and the weakest external radiation field (no or weak emission lines). Consequently the cooling is less dramatic and particles can be present with energies high enough to produce synchrotron emission extending to soft X-ray energies and TeV radiation through the SSC process. Being the inverse Compton cooling ineffective, the Compton dominance is expected to be small;

(ii) LBL are intrinsically more powerful than HBL and in some cases the external field can be responsible for most of the cooling. The stronger cooling limits the particle energy implying that the synchrotron and inverse Compton emission peak at lower frequencies, in the optical and GeV bands, respectively, with a larger Compton dominance parameter;

(iii) FSRQ represent the most powerful blazars, where the contribution from the external radiation to the cooling is the

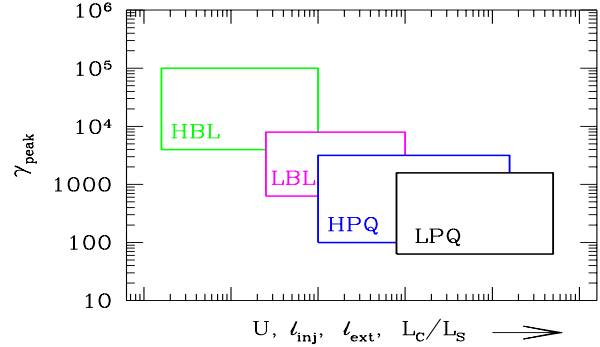


Figure 7. Schematic representation of the proposed unifying scheme: the sequence HBL, LBL, HPQ, LPQ corresponds to an increase in the external radiation field, the total energy density and the injected power. These in turn result in a decrease of γ_{peak} and an increase in the Compton dominance.

greatest. The emission by synchrotron and EC cannot extend at frequencies larger than the IR and MeV–GeV bands and the γ -ray radiation completely dominates the radiative output. Within this class, there is an hint of a further subdivision between low and high polarization objects, with a tendency for LPQ to be more extreme (lower values of γ_{peak} and larger values of $(U_r + U_B)$, ℓ_{inj} and so on).

The correlations among the different quantities ensure that the knowledge of one of them allows to estimate the entire spectral energy distribution, and also the probable classification of the object. This is of course of great relevance for the study at high energies of those blazars not detected so far in the γ -ray band and the consequences on their variability patterns and duty cycles. Finally, the above findings have to be taken into account when considering the absorption of high energy radiation by the diffuse background fields as well as the estimates on the blazar contribution to the γ -ray background.

In the currently most accepted unification schemes for radio-loud sources, weak and powerful blazars are the beamed counterparts of Fanaroff–Riley type I (FR I, Fanaroff & Riley 1974) and type II (FR II) radio galaxies, respectively. Indeed continuity in the properties of blazars along a power sequence has been suggested by Maraschi & Rovetti (1994), Sambruna et al. (1996) and Fossati et al. (1997) on the basis of statistical arguments. Within this frame, the blazar sequence would therefore manifest itself in several observational properties, including the total source power, the luminosity in emission lines, the extended radio power, the dominance of γ -rays over the other spectral components and the broad band shape of the SED (see Fig. 7). We therefore provide evidence for the unification of all radio-loud sources and suggest a deeper physical understanding for it, based on the total power generated in the very central engine of these spectacular sources.

ACKNOWLEDGMENTS

Thanks are due to the Italian MURST (Annalisa Celotti, GF) and the Institute of Astronomy PPARC Theory Grant

(Annalisa Celotti) for financial support. Andrea Comastri acknowledges financial support from the Italian Space Agency under contract ARS-96-70 This research has made use of the NASA/IPAC extragalactic database (NED), which is operated by the Jet Propulsion Laboratory, California Institute of Technology, under contract with the National Aeronautic and Space Administration.

REFERENCES

- Adam G., 1985, *A&AS*, 61, 225 (A85)
- Aller H.D., Aller M.F., Latimer G.E., Hodge, P.E., 1985, *ApJS*, 59, 513 (A185)
- Bersanelli M., Bouchet P., Falomo R., Tanzi E.G., 1992, *AJ*, 104, 28 (Be92)
- Bertsch D.L. et al., 1993, *ApJ*, 405, L21 (Be93)
- Biermann P.L., Kuhr H., Snyder W.A., Zensus J.A., 1987, *A&A*, 85, 9 (Bi87)
- Blandford R.D., 1993, in Friedlander M., Gehrels N., Macomb D.J., eds, *Proc. CGRO AIP 280*. New York, p. 533
- Blandford R.D., Levinson A., 1995, *ApJ*, 441, 79
- Bloom S.D., Marscher A.P., 1991, *ApJ*, 366, 16 (BM91)
- Bloom S.D., Marscher A.P., 1993, in Friedlander M., Gehrels N., Macomb D.J., eds, *Proc. CGRO AIP 280*. New York, p. 578
- Bloom S.D., Marscher A.P., Gear W.K., Terasanta H., Valtaoja E., Aller H.D., Aller M.F., 1994, *AJ*, 108, 398 (BM94)
- Boroson T.A. & Green R., 1992, *ApJS*, 80, 109
- Bozayan E.P., Hemenway P.D., Argue A.N., 1990, *AJ*, 99, 1421 (Bo90)
- Bregman J.N., Glassgold A.E., Huggins P.J., Kinney A.L., 1985, *ApJ*, 291, 505 (B85)
- Breslin A.C. et al., 1997, *IAUC 6592* (B97)
- Brinkmann W., Siebert J., Boller T., 1994, *A&A*, 281, 355 (B94)
- Brinkmann W., Siebert J., Reich W., Furst E., Reich P., Voges W., Trumper J., Wielebinski R., 1995, *A&AS*, 109, 147 (B95)
- Cappi M., Comastri A., Molendi S., Palumbo G.C.C., Della Ceca R., Maccacaro T., 1994, *MNRAS*, 271, 438
- Catanese M. et al., 1997a, *ApJ*, 480, 562 (Ca97)
- Catanese M. et al., 1997b, proceedings of 25th ICRC (Durban), in press (Cat97)
- Celotti A., Padovani P., Ghisellini G., 1997, *MNRAS*, 286, 415
- Chini R., Biermann P.L., Gemund H.-P., 1989, *A&A*, 221, L3 (Ch89)
- Clegg P.E. et al., 1983, *ApJ*, 273, 58 (C83)
- Collmar, W., 1996, in *Gamma ray emitting AGN*, MPI H-V37-1996 eds. J.G. Kirk, M. Camenzind, C. von Montigny & S. Wagner, p. 9 (Co97)
- Comastri A., Fossati G., Ghisellini G., Molendi S., 1997, *ApJ*, 480, 534 (C97)
- Condon J.J., Hicks P.D., Jauncey D.L., 1977, *AJ*, 82, 692 (Co77)
- Condon J.L., Anderson E., Broderick J.J., 1995, *AJ*, 109, 2318 (Co95)
- Dermer C.D., 1995, *ApJ*, 446, L63
- Dermer C.D., Schlickeiser R., 1993, *ApJ*, 416, 458
- Dingus B.L. et al., 1996, *ApJ*, 467, 589 (Di96)
- Dondi L. & Ghisellini G., 1995, *MNRAS*, 273, 583
- Edelson R.A., 1994, *AJ*, 94, 1150 (E94)
- Elvis M., Plummer D., Schachter J., Fabbiano G., 1992, *ApJS*, 79, 331 (E92)
- Falomo R., Scarpa R., Bersanelli M., 1994, *ApJS*, 93, 125 (F94)
- Fanaroff B.L., Riley J.M., 1974, *MNRAS*, 167, 31
- Fichtel C.E. et al., 1994, *ApJS*, 94, 551
- Fossati G., Maraschi L., Celotti A., Comastri A., Ghisellini G., 1998, *MNRAS*, in press
- Fossati G., Celotti A., Ghisellini G. & Maraschi, L., 1997, *MNRAS*, 289, 136
- Fricke K.J., Kollatschny W., Witzel A., 1983, *A&A*, 117, 60 (Fr83)
- Giommi P., Ansari S.G., Micol A., 1995, *A&AS*, 109, 267
- Gear W.K. et al., 1994, *MNRAS*, 267, 167 (G94)
- Ghisellini G., 1989, *MNRAS*, 238, 449
- Ghisellini G., Madau P., 1996, *MNRAS*, 280, 67
- Ghisellini G., Maraschi L., 1989, *ApJ*, 340, 181
- Ghisellini G., Maraschi L., 1994, in Fichtel C.E., Gehrels N., Norris J.P., eds, *The Second Compton Symp.*, AIP 304. New York, p. 616
- Ghisellini G., Maraschi L., Tanzi E., Treves A., 1986, *ApJ*, 310, 317 (G86)
- Ghisellini G., Maraschi L., Dondi L., 1996, *A&AS*, 120, 503
- Ghisellini G. et al., 1997, *A&A*, in press (G97)
- Glass I.S., 1981, *MNRAS*, 194, 795 (G81)
- Hartmann R.C. et al. 1993, *ApJ*, 407, L41 (Ha93)
- Hunter S.D. et al., 1993, *A&A*, 272, 59 (H93)
- Impey C.D., Neugebauer G., 1988, *AJ*, 95, 307 (IN88)
- Impey C.D., Tapia S., 1988, *ApJ*, 333, 666 (IT88)
- Impey C.D., Tapia S., 1990, *ApJ*, 354, 124 (IT90)
- Kühr H., Witzel A., Pauliny-Toth I.I.K., Nauber U., 1981, *A&AS*, 45, 367 (K81)
- Landau R., Jones T.W., Epstein E.E., Neugebauer G., Soifer B.T., Werner M.W., Puschell J.J., Balonek T.J., 1983, *ApJ*, 268, 68 (L83)
- Landau R. et al., 1986, *ApJ*, 308, 78 (L86)
- Lawrence A., Rowan-Robinson M., Efstathiou A., Ward M.J., Elvis M., Smith M.G., Duncan W.D., Robson E.I., 1991, *MNRAS*, 248, 91 (L91)
- Lawson A.J., Turner M.J.L., 1997, *MNRAS*, 288, 920 (LT97)
- Ledden J.F., O'Dell S.L., 1985, *ApJ*, 298, 630 (Le85)
- Lin Y.C. et al., 1995, *ApJ*, 442, 96 (L95)
- Lin Y.C. et al., 1996, *ApJS*, 105, 331 (L96)
- Litchfield S.J., Robson E.I., Stevens J.A., 1994, *MNRAS*, 270, 341 (Li94)
- Lorenzetti D., Massaro E., Perola G.C., Spinoglio L., 1990, *A&A*, 235, 35 (L90)
- McNaron-Brown K. et al., 1995, *ApJ*, 451, 575 (Mc95)
- Macomb D.J. et al., 1995, *ApJ*, 449, L99 (Ma95)
- Macomb D.J. et al., 1996, *ApJ*, 459, L111 (Erratum) (Ma96b)
- Madejski G., Takahashi T., Tashiro M., Kubo H., Hartman R., Kallman T., Sikora M., 1996, *ApJ*, 459, 156 (Ma96)
- Mannheim K., 1993, *A&A*, 269, 67
- Maraschi L., Rovetti F., 1994, *ApJ*, 436, 79
- Maraschi L., Schwartz D.A., Tanzi E.G., Treves A., 1985, *ApJ*, 294, 615 (Ma85)
- Maraschi L., Ghisellini G., Celotti A., 1992, *ApJ*, 397, L5
- Maraschi L. et al. 1994, *ApJ*, 435, L91 (Ma94)

- Maraschi L., Fossati G., Tagliaferri G., Treves A., 1995, *ApJ*, 443, 578
- Mattox J.R. et al., 1993, *ApJ*, 410, 609 (M93)
- Mattox J.R., Wagner S.J., Malkna M., McGlynn T.A., Schachter J.F., Grove J.E., Johnson W.N., Kurfess J.D., 1997, *ApJ*, 476, 692 (M97)
- Mattox J.R., Schachter J., Molnar L., Hartman R.C., Patnaik A.R., 1997, *ApJ*, 481, 95
- Mukherjee R. et al., 1995, *ApJ*, 445, 189 (Mu95)
- Mukherjee R. et al., 1996, *ApJ*, 470, 831 (Mu96)
- Nolan P.L. et al., 1993, *ApJ*, 414, 82 (N93)
- Nolan P.L. et al., 1996, *ApJ*, 459, 100 (N96)
- Netzer H. et al., 1996, *MNRAS*, 279, 429 (Ne96)
- Padovani P., Giommi P., 1995, *ApJ*, 444, 567
- Perley R.A., 1982, *AJ*, 87, 859 (P82)
- Perlman E.S. et al., 1996, *ApJS*, 104, 251 (P96)
- Petry D. et al., 1996, *A&A*, 311, L13
- Pian E. et al., 1993, *ApJ*, 416, 130 (Pi93)
- Pian E., Falomo R., Scarpa R., Treves A., 1994, *ApJ*, 37, 152 (Pi94)
- Pian E., Falomo R., Ghisellini G., Maraschi L., Sambruna R.M., Scarpa R., Treves A., 1996, *ApJ*, 459, 169 (Pi96)
- Pica A.J., Smith A.G., Webb J.R., Leacock R.J., Clements S., Gombola P.P., 1988, *AJ*, 96, 1215 (P88)
- Pohl M., Reich W., Schlickeiser R., Reich P., Ungerechts H., 1996, *A&AS*, 120, 529 (Po96)
- Quinn J. et al., 1996, *ApJ*, 456, L83 (Q96)
- Radecke H.-D. et al., 1995, *ApJ*, 438, 659 (R95)
- Raiteri C.M. et al., 1997, *A&AS*, in press (Ra97)
- Reuter H.-P. et al., 1997, *A&AS*, 122, 271 (R97)
- Rieke G.H., Lebofsky M.J., Wiśniewski W.Z., 1982, *ApJ*, 263, 73 (R82)
- Rybicki G.B. & Lightman A.P., 1979, *Radiative processes in Astrophysics*, J. Wiley & Sons (New York)
- Robson E.I., Gear W.K., Brown L.M.J., Courvoisier T.J.-L., Smith M.G., 1986, *Nat*, 323, 134 (R86)
- Sambruna R.M., Barr P., Giommi P., Maraschi L., Tagliaferri G., Treves A., 1994, *ApJS*, 95, 371 (Sa94)
- Sambruna R.M. et al., 1997, *ApJ*, 474, 639 (Sa97)
- Schonfelder V., 1994, *ApJS*, 92, 593 (Sh94)
- Sikora M., Begelman M.C., Rees M.J., 1994, *ApJ*, 421, 153
- Sitko M.L., Junkkarinen V.T., 1985, *PASP*, 97, 1158
- Sitko M.L., Sitko A.K., 1991, *PASP*, 103, 160 (Si91)
- Smith P.S., Elston R., Berriman G., Allen R.G., Balonek T.J., 1988, *ApJ*, 326, L39 (Sm88)
- Sreekumar P. et al., 1996, *ApJ*, 464, 628 (Sr96)
- Stacy J.C., Vestrand W.T., Sreekumar P., Bonnell J., Kubo H., Hartman R.C., 1996, *A&AS*, 120, 549 (Sta96)
- Steppe H., Salter C.J., Chini R., Kraysa E., Brunswig W., Lobato Perez J., 1988, *A&AS*, 75, 317 (St88)
- Steppe H., Liechti S., Mauersberger R., Kompe C., Brunswig W., Ruiz-Moreno M., 1992, *A&AS*, 96, 441 (St92)
- Steppe H. et al., 1993, *A&AS*, 102, 611 (St93)
- Stevens J.A., Litchfield S.J., Robson E.I., Hughes D.H., Gear W.K., Terasranta H., Valtaoja E., Tornikoski M., 1994, *ApJ*, 437, 91 (S94)
- Stickel M., Fried J.W., Kühr H., 1993, *A&AS*, 98, 393
- Stickel M., Meisenheimer K., Kühr H., 1994, *A&AS*, 105, 211 (St94)
- Stickel M., Rieke G.H., Kühr H., Rieke M.J., 1996, *ApJ*, 468, 556 (St96)
- Terasranta H. et al., 1989, *A&AS*, 75, 317 (T89)
- Terasranta H. et al., 1992, *A&AS*, 94, 121 (T92)
- Thompson D.J. et al., 1993, *ApJ*, 415, L13 (T93)
- Thompson D.J. et al., 1995, *ApJS*, 101, 259 (T95)
- Thompson D.J. et al., 1996, *ApJS*, 107, 227 (T96)
- Tornikoski M., Valtaoja E., Terasranta H., Lainela M., Bramwell D., Botti L.C.L., 1993, *AJ*, 105, 1680 (To93)
- Tornikoski M. et al., 1996, *A&AS*, 116, 157 (To96)
- Tosti G. et al., 1997, *A&AS*, submitted (To97)
- Turner M.J.L. et al., 1990, *MNRAS*, 244, 310 (T90)
- Urry M.C., Padovani P., 1995, *PASP*, 107, 803
- Urry C.M., Sambruna R.M., Worrall D.M., Kollgaard R.I., Feigelson E.D., Perlman E.S., Stocke J.T., 1996, *ApJS*, 463, 424 (U96)
- Urry C.M. et al. 1997, *ApJ*, in press (U97)
- Valtaoja E., Lahtenmaki A., Terasranta H., 1992, *A&AS*, 95, 73 (V92)
- Vermeulen R.C., Ogle P.M., Tran H.D., Browne I.W.A., Cohen M.H., Readhead, A.C.S., Taylor G.B. & Goodrich R.W., 1995, *ApJ*, 425, L5
- Vestrand W.T., Stacy J.G., Sreekumar P., 1996, *ApJ*, 454, L93 (V96)
- Villata M. et al., 1997, *A&AS*, 121, 119 (V97)
- von Montigny C. et al., 1995, *ApJ*, 440, 525 (vM95)
- von Montigny C. et al., 1997, *ApJ*, in press
- Wagner S., Sanchez-Pons F., Quirrenbach A., Witzel A., 1990, *A&A*, 235, L1 (W90)
- Wagner S.J. et al., 1995, *A&A* 298, 688
- Wagner S.J. et al., 1995, *ApJ*, 454, L97 (W95)
- Wagner S.J. et al., 1996, *AJ*, 111, 2187 (W96)
- Wall J.V., Peacock J.A., 1985, *MNRAS*, 216, 173 (WP85)
- Webb J.R., Smith A.G., Leacock R.J., Fitzgibbons G.L., Gombola P.P., Shepherd D.W., 1988, *AJ*, 95, 374 (W88)
- Webb J.R., Barnello T., Robson I., Hartman R.C., 1995, *IAUC* 6168 (We95)
- Weekes T.C. et al., 1996, *A&AS*, 120, 603
- Wilkes B.J., Tananbaum H., Worrall D.M., Avni Y., Oey M.S., Flanagan J., 1994, *ApJS*, 92, 53 (Wi94)
- Wiren S., Valtaoja E., Terasranta H., Kotilainen J., 1992, *AJ*, 104, 111 (W92)
- Worrall D.M., Wilkes B.J., 1990, *ApJ*, 360, 396 (WW90)
- Worrall D.M., Giommi P., Tananbaum H., Zamorani G., 1987, *ApJ*, 313, 596 (W87)
- Wright A.E., Wark R.M., Troup E., Otrupcek R., Jennings D., Hunt A., Andcooke D.J., 1991, *MNRAS*, 251, 330 (W91)

APPENDIX

Table 1. List of sources. (1),(2) Source names; (3) redshift; (4) classification: HPQ and LPQ stand for highly and lowly polarized quasars, while NP indicates sources with no polarization measure; HBL, LBL and IBL refer to high, low and intermediate frequency BL Lacs, respectively; (5) references to the data of Fig. 1.

Source (1)	Other name (2)	z (3)	Class. (4)	Refs. for data (5)
0202+149	4C 15.05	0.833	HPQ	B85, BM94, C97, IT90, K81, NED, St92, St96, vM95
0208-512	PKS	1.003	HPQ	Be93, C97, IT88, NED, Sta96, To96
0219+428	3C 66A	0.444	LBL	C97, Di96, G86, NED, Pi93, Si91, T95, WW90
0234-285	CTD 20	1.213	HPQ	B95, BM91, E94, K81, NED, P82, St93, T92, vM95
0235+164	AO	0.940	LBL	BM94, E94, G94, H93, K81, Ma96, NED, Pi93, S94, Si91, To96, WW90
0420-014	PKS	0.915	HPQ	BM94, Ch89, Co95, E94, IN88, K81, Li94, NED, Ra97, R95, S94, Si91, Sm88, To96, WW90
0440-003	NRAO 190	0.844	HPQ	Bo90, K81, NED, St88, T95, To93, To96, W87, WP85
0446+112	PKS	1.207	NP	NED, St88, T95, To96, W92
0454-463	PKS	0.858	LPQ	B94, Fr83, IT90, K81, NED, To96, vM95, W91, WP85
0521-365	PKS	0.055	HPQ	C97, IN88, NED, Pi93, Pi94, Pi96, T95, To96
0528+134	OG 147	2.07	LPQ	B85, BM94, Co77, Co96, E94, IT90, Mc95, Mu96, NED, Po96, R82, R97, Sa97, V92, WP85
0537-441	PKS	0.896	LBL	Be92, C97, IN88, K81, L96, Ma85, NED, Pi93, Sa94, WP85, WW90
0716+714	S5	>0.3	LBL	BM94, C94, E94, G97, IN88, K81, L95, NED, St92, W96
0735+178	PKS	>0.424	LBL	C97, E94, G94, IN88, NED, N96, Pi93, Si91, To96, WW90
0804+499	OJ 508	1.433	HPQ	BM94, C97, NED, St94, vM95
0805-077	PKS	1.837	NP	K81, NED, St93, T95
0827+243	OJ 248	2.05	LPQ	B95, BM94, NED, Ra97, To96, V97, vM95
0836+710	4C 71.07	2.172	LPQ	BM94, C97, E92, E94, K81, NED, Ra97, T93, W90, W92, WP85
0917+449	S4	2.18	LPQ	BM94, C97, E94, NED, St93, T95
0954+556	4C55.17	0.901	HPQ	BM94, C97, G94, K81, NED, Sr96
0954+658	S4	0.368	LBL	C97, G94, IN88, K81, L86, Mu95, NED, St88
1101+384	Mkn 421	0.031	HBL	Ma95, Ma96b
1127-145	PKS	1.187	LPQ	A85, B94, Bo90, E94, IT90, K81, NED, Sr96, To96
1156+295	4C 29.45	0.729	HPQ	BM94, E94, G94, IN88, Le85, Li94, LT96, NED, Pi93, Ra97, S94, Sa94, Si91, To96, V97, vM95, We95
1219+285	ON 231	0.102	LBL	BM91, C97, E92, E94, IN88, Lo90, NED, Pi93, Si91, To97, vM95, WW90
1222+216	4C 21.35	0.435	LPQ	B95, NED, Sr96, To96
1226+023	3C 273	0.158	LPQ	A185, C83, G94, IN88, K81, L83, Mc95, NED, R86, Sh94, T90
1229-021	PKS	1.045	LPQ	K81, NED, P88, Ra97, Sr96, St88, St94, To96, Wi94
1253-055	3C 279	0.538	HPQ	Ma94
1313-333	PKS	1.210	NP	N96, NED, St88, St92, St94, To96
1406-076	PKS	1.494	LPQ	NED, St88, To93, To96, W95
1424-418	PKS	1.522	HPQ	G81, IN88, NED, To96, T96
1510-089	PKS	0.361	HPQ	C97, E94, G81, G94, IN88, K81, L86, LT97, NED, Pi93, Ra97, Sa94, Si91, Sm88, Sr96, St93, To96, V97, WP85

Table 1. *continue*

Source (1)	Other name (2)	z (3)	Class. (4)	Refs. for data (5)
1604+159	4C15.54	0.357	LBL	GAM95, IN88, Le85, NED, Sr96
1606+106	4C 10.45	1.227	LPQ	B95, Bi87, BM94, E94, IT90, K81, NED, To96, vM95
1611+343	DA 406	1.404	LPQ	C97, E94, G94, K81, NED, Ra97, vM95
1622-253	PKS	0.786	LPQ	N96, NED, St94
1622-297	PKS	0.815	LPQ	K81, M97, NED, St93
1633+382	4C 38.41	1.814	LPQ	BM91, BM94, Bo90, C97, IN88, K81, M93, Ra97, V92, V97, WP85
1652+398	Mkn 501	0.055	HBL	B97, BM91, C97, G94, IN88, L91, Pi93, Q96, Sa94, St88, W92, WW90
1730-130	NRAO 530	0.902	NP	B94, BM91, E94, N96, NED, St88, St93, To96, W88
1739+522	4C 51.37	1.375	HPQ	B95, BM91, K81, NED, St88, St93, St94, V92, vM95
1741-038	OT-68	1.054	HPQ	B94, E94, G94, K81, NED, St88, St92, St93, St94, To96, vM95
1933-400	PKS	0.966	NP	B94, Di96, K81, NED, St94, To96
2032+107	PKS	0.601	LBL	Di96, GAM95, NED, WW90
2052-474	PKS	0.071	LPQ	B94, IT90, K81, NED, To96, vM95
2155-304	PKS	0.117	HBL	U97, V96
2200+420	BL Lac	0.069	LBL	BM94, Ca97, E94, IN88, NED, P96, Pi93, S94, St93, To96, U96
2230+114	CTA 102	1.037	HPQ	B94, BM94, E94, F94, IN88, K81, Le85, Mc95, N93, Ne96, Ra97, St93, T89, To96, W92, Wi94
2251+158	3C 454.3	0.859	HPQ	Be92, BM91, BM94, C97, E94, G94, Ha93, IN88, K81, Le85, Mc95, Ne96, NED, Pi93, Ra97, S94, Sm88
2344+514	1ES	0.044	HBL	Cat97, NED, P96

Table 1. *continue*

A85:	Adam (1985)	A185:	Aller et al. (1985)
B85:	Bregman et al. (1985)	B94:	Brinkmann, Siebert & Boller (1994)
B95:	Brinkmann et al. (1995)	B97:	Breslin et al. (1997)
Be92:	Bersanelli et al. (1992)	Be93:	Bertsch et al. (1993)
Bi87:	Biermann et al. (1987)	BM91:	Bloom & Marscher (1991)
BM94:	Bloom et al. (1994);	Bo90:	Bozayan, Hemenway & Argue (1990);
C83:	Clegg et al. (1983)	C94:	Cappi et al. (1994)
C97:	Comastri et al. (1997)	Ca97:	Catanese et al. (1997a)
Cat97:	Catanese et al. (1997b)	Ch89:	Chini, Biermann & Gemund (1989)
Co77:	Condon, Hicks & Jauncey (1977)	Co95:	Condon, Anderson & Broderick (1995)
Co96:	Collmar (1996)	Di96:	Dingus et al. (1996)
E92:	Elvis et al. (1992)	E94:	Edelson (1994)
F94:	Falomo, Scarpa & Bersanelli (1994)	Fr83:	Fricke, Kollatschny & Witzel (1983)
GAM95:	Giommi, Ansari & Micol (1995):	G81:	Glass (1981)
G86:	Ghisellini et al. (1986)	G94:	Gear et al. (1994)
G97:	Ghisellini et al. (1997)	H93:	Hunter et al. (1993)
Ha93:	Hartmann et al. (1993)	IN88:	Impey & Neugebauer (1988)
IT88:	Impey & Tapia (1988)	IT90:	Impey & Tapia (1990)
K81:	Kühr et al. (1981)	L83:	Landau et al. (1983)
L86:	Landau et al. (1986)	L91:	Lawrence et al. (1991)
L95:	Lin et al. (1995)	L96:	Lin et al. (1996)
Le85:	Ledden & O'Dell (1985)	Li94:	Litchfield, Robson & Stevens (1994)
Lo90:	Lorenzetti et al. (1990)	LT97:	Lawson & Turner (1997)
M93:	Mattox et al. (1993)	M97:	Mattox et al. (1997)
Ma85:	Maraschi et al. (1985)	Ma94:	Maraschi et al. (1994)
Ma95:	Macomb et al. (1995)	Ma96:	Madejski et al. (1996)
Ma96b:	Macomb et al. (1996)	Mc95:	McNaron-Brown et al. (1995)
Mu95:	Mukherjee et al. (1995)	Mu96:	Mukherjee et al. (1996)
N93:	Nolan et al. (1993)	N96:	Nolan et al. (1996)
Ne96:	Netzer et al. (1996)	P82:	Perley (1982)
P88:	Pica et al. (1988)	P96:	Perlman et al. (1996)
Pi93:	Pian et al. (1993)	Pi94:	Pian et al. (1994)
Pi96:	Pian et al. (1996)	Po96:	Pohl et al. (1996)
Q96:	Quinn et al. (1996)	R82:	Rieke, Lebofsky & Wiśniewski (1982)
R86:	Robson et al. (1986)	R95:	Radecke et al. (1995)
R97:	Reuter et al. (1997)	Ra97:	Raiteri et al. (1997)
S94:	Stevens et al. (1994)	Sa94:	Sambruna et al. (1994)
Sa97:	Sambruna et al. (1997)	Sh94:	Schonfelder (1994)
Si91:	Sitko & Sitko (1991)	Sm88:	Smith et al. (1988)
Sr96:	Sreekumar et al. (1996)	St88:	Steppe et al. (1988)
St92:	Steppe et al. (1992)	St93:	Steppe et al. (1993)
St94:	Stickel, Meisenheimer & Kuhr (1994)	St96:	Stickel et al. (1996)
Sta96:	Stacy et al. (1996)	T89:	Terasranta et al. (1989)
T90:	Turner et al. (1990)	T92:	Terasranta et al. (1992)
T93:	Thompson et al. (1993)	T95:	Thompson et al. (1995)
T96:	Thompson et al. (1996)	To93:	Tornikoski et al. (1993)
To96:	Tornikoski et al. (1996)	To97:	Tosti et al. (1997)
U96:	Urry et al. (1996)	U97:	Urry et al. (1997)
V92:	Valtaoja, Lahteenmaki & Terasranta (1992)	V96:	Vestrand et al. (1996)
V97:	Villata et al. (1997)	vM95:	von Montigny et al. (1995)
W87:	Worrall et al. (1987)	W88:	Webb et al. (1988)
W90:	Wagner et al. (1990)	W91:	Wright et al. (1991)
W92:	Wiren et al. (1992)	W95:	Wagner et al. (1995)
W96:	Wagner et al. (1996)	We95:	Webb et al. (1995)
Wi94:	Wilkes et al. (1994)	WP85:	Wall & Peacock (1985)
WW90:	Worrall & Wilkes (1990)		

Table 2. The input parameters for the EC and SSC models are reported in the first and second line for each source, respectively. (1) Source name; (2) region size in units of 10^{15} cm; (3), (4) compactnesses in injected particles and external radiation field; (5) maximum energy of the injected particles; (6) energy of the peak of the stationary electron distribution; (7) spectral index of the injected particles; (8) magnetic field intensity (in Gauss); (9) relativistic Doppler factor. The SSC model for 1253–055 requires monoenergetic injection.

Source (1)	$R/10^{15}$ (2)	ℓ_{inj} (3)	ℓ_{ext} (4)	γ_{max} (5)	γ_{peak} (6)	s (7)	B (8)	δ (9)
0202+149	30	0.05	2	3.0e3	2.5e2	3.0	3.040	14
	80	0.01	–	4.0e4	1.0e4	3.3	0.026	18
0208–512	70	0.02	0.06	7.0e3	1.0e3	3.8	0.563	23
	50	0.08	–	3.0e4	1.5e4	2.0	0.106	16
0219+428	20	0.03	3e-3	1.0e5	8.0e3	2.4	2.040	13.5
	40	0.01	–	2.0e5	1.0e4	2.4	0.590	15
0234–285	40	0.06	1	1.0e4	2.0e2	2.9	4.080	16
	50	0.08	–	6.0e4	1.0e4	3.0	0.067	13
0235+164	50	0.05	0.03	8.0e4	3.0e3	3.0	0.912	20
	60	0.02	–	3.0e5	1.0e4	2.9	0.215	21
0420–014	50	0.03	0.04	1.0e4	2.0e3	3.5	0.745	16
	80	0.01	–	8.0e4	1.5e4	3.0	0.034	20
0440–003	50	0.025	0.025	2.0e4	2.0e3	3.0	0.680	17
	70	0.01	–	8.0e4	2.0e4	3.0	0.106	20
0446+112	50	0.08	1	4.0e3	1.5e2	2.0	0.810	20
	90	0.08	–	1.0e5	1.0e4	3.5	0.011	20
0454–463	30	0.03	0.08	8.0e3	6.0e2	2.1	1.050	16
	80	7e-3	–	8.0e4	3.0e4	2.5	0.018	20
0521–365	50	1.00	0.10	5.0e4	2.0e3	2.5	3.141	1.4
	50	0.60	–	7.0e4	3.5e3	2.7	2.580	1.6
0528+134	65	0.90	7	6.0e3	3.0e2	2.6	6.198	15
	60	0.60	–	8.0e4	3.0e3	3.0	0.215	19
0537–441	70	0.04	1e-3	7.0e4	4.0e3	2.2	0.325	15
	50	0.05	–	1.0e5	4.0e3	2.5	0.430	15
0716+714	30	0.02	7e-3	3.0e4	2.0e3	2.6	1.813	11.5
	50	3e-3	–	5.0e4	4.0e3	2.7	0.460	15
0735+178	40	0.01	4e-3	3.0e4	3.0e3	3.0	0.833	14
	50	3e-3	–	4.0e4	5.0e3	3.3	0.408	17
0804+499	50	0.10	0.70	8.0e3	4.0e2	3.1	3.333	15
	70	0.06	–	8.0e4	1.0e4	3.4	0.073	17
0805–077	40	0.20	2	6.0e3	4.0e2	2.5	2.483	17
	90	0.09	–	1.0e5	9.0e3	3.7	0.037	20
0827+234	50	0.20	0.90	8.0e3	3.0e2	2.3	4.711	16
	70	0.20	–	8.0e4	5.0e3	2.7	0.563	16
0836+710	50	0.70	6.00	7.0e3	1.8e2	3.1	8.814	18
	70	0.30	–	5.0e4	4.0e3	3.0	0.282	17
0917+449	30	0.50	8	6.0e3	2.0e2	2.1	2.267	13
	90	0.03	–	1.0e5	4.0e3	2.3	0.025	23
0954+556	50	0.01	0.02	1.5e4	5.0e3	1.7	0.527	15
	70	4e-3	–	7.0e4	1.0e4	0.0	0.056	17
0954+658	30	4.5e-3	0.025	6.0e3	9.0e2	3.6	2.040	13
	60	7e-4	–	7.0e4	2.0e4	2.0	0.025	18
1101+384	5	6e-3	1e-3	8.0e5	6.0e4	2.0	0.222	11
	10	2e-3	–	8.0e5	2.0e5	1.2	0.093	12
1127–145	60	0.15	0.80	8.0e3	3.0e2	2.3	1.862	15.5
	70	0.10	–	8.0e4	1.5e4	2.3	0.048	17
1156+295	20	0.15	0.08	1.0e4	3.0e3	2.4	1.360	15
	70	0.02	–	8.0e4	9.0e3	2.0	0.252	18
1219+285	20	1.e-3	4.e-3	1.0e5	5.0e3	4.2	1.178	11
	70	5.e-5	–	7.0e4	4.0e4	0.0	0.036	20
1222+216	10	0.10	0.25	8.0e3	3.5e2	2.9	3.333	11
	40	0.02	–	4.0e4	9.0e3	3.2	0.068	11
1226+023	10	1.00	1.50	1.0e4	8.0e1	3.2	8.900	6.5
	40	0.06	–	3.0e4	3.5e3	3.2	0.456	7.0

Table 2. *continue*

Source (1)	$R/10^{15}$ (2)	ℓ_{inj} (3)	ℓ_{ext} (4)	γ_{max} (5)	γ_{peak} (6)	s (7)	B (8)	δ (9)
1229–021	40	0.08	1.00	8.0e3	3.0e2	3.8	2.356	12
	50	0.03	–	2.0e4	1.0e4	4.0	0.105	16
1253–055	30	0.04	0.07	7.0e3	8.0e2	3.2	1.360	18
	80	0.04	–	2.0e4	2.0e4	–	0.059	15
1313–333	40	0.03	0.70	9.0e3	1.0e3	1.9	1.180	17
	70	0.01	–	1.0e5	3.0e4	1.0	0.009	20
1406–076	60	0.05	0.10	1.0e4	3.0e3	1.5	1.080	21
	70	0.08	–	6.0e4	1.5e4	2.3	0.206	18
1424–418	30	0.50	1.00	6.0e3	2.0e2	2.7	4.060	15
	90	0.07	–	1.0e5	5.0e3	3.0	0.093	20
1510–089	20	0.05	0.80	1.0e4	1.2e2	3.3	5.890	13
	30	4e-3	–	3.0e4	4.0e3	2.2	0.061	18
1604+159	20	0.01	0.10	1.0e4	9.0e2	2.1	0.960	15
	50	2e-3	–	7.0e4	3.0e4	2.1	0.011	18
1606+106	30	0.30	3.00	5.0e3	1.5e2	3.0	3.330	15
	70	0.06	–	3.0e4	1.0e4	3.0	0.028	18
1611+343	30	0.20	1.00	5.0e3	2.0e2	2.6	3.041	16
	50	0.20	–	6.0e4	1.3e4	3.3	0.105	13.5
1622–253	30	0.03	0.30	6.0e3	3.0e2	2.5	1.670	15
	70	0.01	–	8.0e4	2.0e4	2.3	0.013	16
1622–297	20	0.10	1.00	2.5e3	6.0e2	1.5	2.150	23
	80	0.03	–	5.0e4	3.0e4	2.1	0.007	21
1633+382	60	0.18	0.60	6.0e3	1.5e3	1.5	1.667	21
	80	0.20	–	7.0e4	2.0e4	2.0	0.052	19
1652+398	5	2e-3	5e-4	8.0e5	1.0e4	2.8	1.110	10
	10	1e-3	–	8.0e5	2.0e4	3.0	0.497	10
1730–130	30	0.04	0.40	3.0e4	4.0e2	2.8	5.440	17
	60	0.02	–	6.0e4	6.0e3	2.4	0.192	16
1739+522	60	0.03	0.08	1.0e4	4.0e2	2.2	0.450	20
	70	0.04	–	1.0e5	2.0e4	2.1	0.019	19
1741–038	60	0.05	0.90	8.0e3	2.5e2	3.8	2.150	17
	60	0.05	–	2.0e4	1.0e4	3.0	0.048	17.5
1933–400	20	0.07	1.00	6.0e3	3.0e2	2.6	4.410	14
	50	0.03	–	5.0e4	8.0e3	2.9	0.060	14
2032+107	20	0.06	0.20	6.0e3	3.0e2	3.0	3.850	12
	50	5e-3	–	5.0e4	4.0e3	3.3	0.118	20
2052–474	50	0.20	2.00	7.0e3	2.0e2	2.8	1.920	15
	70	0.10	–	5.0e4	8.0e3	2.9	0.073	16
2155–304	20	2e-3	3e-4	4.0e5	8.0e3	2.4	1.050	17
	20	2e-3	–	1.0e6	7.0e3	2.6	1.216	18
2200+420	8	8e-3	3e-4	3.0e5	2.7e3	2.8	1.670	10
	20	2e-3	–	3.0e5	5.0e3	2.8	0.430	11
2230+114	40	0.80	5.00	1.0e4	1.0e2	3.1	8.600	10
	70	0.03	–	3.0e4	6.0e3	2.9	0.077	18
2251+158	40	0.80	5.00	6.0e3	1.0e2	2.3	7.450	10
	70	0.04	–	6.0e4	4.0e3	2.2	0.073	18
2344+512	8	1.4e-4	1e-4	7.0e5	4.0e4	3.7	0.470	14
	10	2e-4	–	8.0e5	4.5e4	3.5	0.220	13

Table 3. Linear correlations for the EC model. (1), (2), (4), (5) parameters of the correlation of the form $y = mx + q$; (3) number of objects; (6) correlation coefficient; (7) probability of a random distribution; (8) sources considered.

y (1)	x (2)	N (3)	m (4)	q (5)	r (6)	P (7)	Objects (8)
$\log \gamma_{\text{peak}}$	$\log(U_r + U_B)$	51	-0.63 ± 0.04	2.97 ± 0.04	0.902	7.2×10^{-10}	All
		37	-0.50 ± 0.06	2.88 ± 0.05	0.812	2.5×10^{-9}	Only FSRQ
		14	-0.80 ± 0.12	2.88 ± 0.14	0.886	2.4×10^{-5}	Only BL Lacs
$\log \gamma_{\text{peak}}$	$\log U_B$	51	-0.64 ± 0.09	2.33 ± 0.10	0.735	2.3×10^{-9}	All
		37	-0.43 ± 0.08	2.33 ± 0.08	0.676	4.5×10^{-6}	Only FSRQ
		14	-0.67 ± 0.19	2.70 ± 0.28	0.719	3.7×10^{-3}	Only BL Lacs
$\log \gamma_{\text{peak}}$	$\log U_r$	51	-0.56 ± 0.04	2.89 ± 0.04	0.911	1.2×10^{-10}	All
		37	-0.50 ± 0.06	2.85 ± 0.05	0.818	7.9×10^{-11}	Only FSRQ
		14	-0.64 ± 0.10	2.82 ± 0.15	0.875	4.0×10^{-5}	Only BL Lacs
$\log \gamma_{\text{peak}}$	$\log \ell_{\text{ext}}$	51	-0.48 ± 0.04	2.47 ± 0.05	0.890	7.1×10^{-10}	All
		37	-0.54 ± 0.07	2.47 ± 0.05	0.799	1.6×10^{-9}	Only FSRQ
		14	-0.49 ± 0.11	2.39 ± 0.29	0.794	7.0×10^{-4}	Only BL Lacs
$\log \gamma_{\text{peak}}$	$\log \ell_{\text{inj}}$	51	-0.61 ± 0.08	2.11 ± 0.12	0.735	3.4×10^{-9}	All
		37	-0.41 ± 0.12	2.23 ± 0.14	0.491	2.0×10^{-3}	Only FSRQ
		14	-0.48 ± 0.21	2.59 ± 0.48	0.566	3.5×10^{-2}	Only BL Lacs
$\log \gamma_{\text{peak}}$	$\log(\ell_{\text{inj}} + \ell_{\text{ext}})$	51	-0.58 ± 0.05	2.54 ± 0.06	0.871	1.7×10^{-10}	All
		37	-0.55 ± 0.09	2.54 ± 0.05	0.740	1.7×10^{-7}	Only FSRQ
		14	-0.61 ± 0.14	2.49 ± 0.29	0.776	1.1×10^{-3}	Only BL Lacs
$\log \gamma_{\text{peak}}$	$\log L_C/L_{\text{syn}}$	51	-0.70 ± 0.11	3.53 ± 0.12	0.690	2.2×10^{-8}	All
		37	-0.44 ± 0.18	3.15 ± 0.23	0.381	2.0×10^{-2}	Only FSRQ
		14	-0.46 ± 0.28	3.67 ± 0.16	0.427	1.3×10^{-1}	Only BL Lacs
$\log L_C/L_{\text{syn}}$	$\log \ell_{\text{inj}}$	51	0.49 ± 0.09	1.54 ± 0.14	0.601	2.3×10^{-6}	All
		37	0.02 ± 0.12	1.18 ± 0.13	0.027	8.7×10^{-1}	Only FSRQ
		14	0.47 ± 0.18	1.15 ± 0.41	0.599	2.4×10^{-2}	Only BL Lacs
$\log L_C/L_{\text{syn}}$	$\log \ell_{\text{ext}}$	51	0.42 ± 0.05	1.28 ± 0.07	0.797	2.2×10^{-9}	All
		37	0.25 ± 0.09	1.27 ± 0.07	0.426	8.6×10^{-3}	Only FSRQ
		14	0.38 ± 0.13	1.07 ± 0.34	0.649	1.2×10^{-2}	Only BL Lacs
$\log L_C/L_{\text{syn}}$	$\log(\ell_{\text{inj}} + \ell_{\text{ext}})$	51	0.50 ± 0.06	1.22 ± 0.07	0.771	6.7×10^{-10}	All
		37	0.20 ± 0.10	1.23 ± 0.07	0.311	6.1×10^{-2}	Only FSRQ
		14	0.55 ± 0.14	1.15 ± 0.28	0.749	2.0×10^{-3}	Only BL Lacs
$\log L_C/L_{\text{syn}}$	$\log L_{\text{inj}}^{\text{obs}}$	51	0.40 ± 0.06	-18.44 ± 2.81	0.702	8.7×10^{-9}	All
		37	0.17 ± 0.08	-7.28 ± 4.03	0.335	4.2×10^{-2}	Only FSRQ
		14	0.29 ± 0.12	-13.44 ± 5.61	0.573	3.2×10^{-2}	Only BL Lacs
$\log L_C/L_{\text{syn}}$	$\log \nu_{\text{peak}}^{\text{obs}}$	51	-0.45 ± 0.06	11.57 ± 1.40	0.736	1.4×10^{-9}	All
		37	-0.25 ± 0.08	6.92 ± 1.93	0.449	5.3×10^{-3}	Only FSRQ
		14	-0.31 ± 0.14	7.88 ± 3.45	0.544	4.4×10^{-2}	Only BL Lacs
$\log L_C/L_{\text{syn}}$	$\log B$	51	0.37 ± 0.24	0.81 ± 0.11	0.217	1.3×10^{-1}	All
		37	-0.15 ± 0.19	1.26 ± 0.09	0.132	4.3×10^{-1}	Only FSRQ
		14	-0.25 ± 0.50	0.14 ± 0.16	0.145	6.2×10^{-1}	Only BL Lacs
$\log \ell_{\text{ext}}$	$\log \ell_{\text{inj}}$	51	1.28 ± 0.13	0.76 ± 0.19	0.822	6.3×10^{-10}	All
		37	0.83 ± 0.16	0.52 ± 0.17	0.671	5.5×10^{-6}	Only FSRQ
		14	0.82 ± 0.31	-0.71 ± 0.71	0.605	2.2×10^{-2}	Only BL Lacs
$\log U_B$	$\log U_r$	51	0.57 ± 0.06	-0.86 ± 0.06	0.812	1.2×10^{-10}	All
		37	0.82 ± 0.08	-1.05 ± 0.07	0.857	5.7×10^{-10}	Only FSRQ
		14	0.54 ± 0.16	-0.69 ± 0.24	0.693	6.0×10^{-3}	Only BL Lacs

Table 4. Linear correlations for the SSC model. (1), (2), (4), (5) parameters of the correlation of the form $y = mx + q$; (3) number of objects; (6) correlation coefficient; (7) probability of a random distribution; (8) sources considered.

y (1)	x (2)	N (3)	m (4)	q (5)	r (6)	P (7)	Objects (8)
$\log \gamma_{\text{peak}}$	$\log(U_r + U_B)$	51	-0.29 ± 0.05	3.37 ± 0.13	0.616	1.5×10^{-6}	All
		37	-0.24 ± 0.05	3.43 ± 0.12	0.627	3.3×10^{-5}	Only FSRQ
		14	-0.36 ± 0.13	3.29 ± 0.31	0.638	1.4×10^{-2}	Only BL Lacs
$\log \gamma_{\text{peak}}$	$\log U_B$	51	-0.15 ± 0.04	3.51 ± 0.15	0.466	5.7×10^{-4}	All
		37	-0.17 ± 0.04	3.35 ± 0.14	0.627	3.2×10^{-5}	Only FSRQ
		14	-0.23 ± 0.11	3.48 ± 0.32	0.524	5.4×10^{-2}	Only BL Lacs
$\log \gamma_{\text{peak}}$	$\log U_r$	51	-0.31 ± 0.05	3.29 ± 0.13	0.642	3.7×10^{-7}	All
		37	-0.25 ± 0.05	3.41 ± 0.13	0.627	3.3×10^{-5}	Only FSRQ
		14	-0.41 ± 0.13	3.07 ± 0.35	0.672	8.5×10^{-3}	Only BL Lacs
$\log \gamma_{\text{peak}}$	$\log \ell_{\text{inj}}$	51	-0.19 ± 0.06	3.70 ± 0.11	0.434	1.5×10^{-3}	All
		37	-0.19 ± 0.08	3.72 ± 0.12	0.365	2.6×10^{-2}	Only FSRQ
		14	-0.36 ± 0.16	3.16 ± 0.45	0.539	4.7×10^{-2}	Only BL Lacs
$\log \gamma_{\text{peak}}$	$\log L_C/L_{\text{syn}}$	51	0.05 ± 0.07	3.96 ± 0.10	0.100	4.8×10^{-1}	All
		37	0.32 ± 0.09	3.52 ± 0.14	0.504	1.5×10^{-3}	Only FSRQ
		14	0.12 ± 0.23	4.09 ± 0.16	0.143	6.2×10^{-1}	Only BL Lacs
$\log L_C/L_{\text{syn}}$	$\log \ell_{\text{inj}}$	51	0.47 ± 0.10	1.94 ± 0.19	0.555	2.4×10^{-5}	All
		37	-0.03 ± 0.14	1.41 ± 0.20	0.031	8.6×10^{-1}	Only FSRQ
		14	0.24 ± 0.23	0.95 ± 0.64	0.292	3.1×10^{-1}	Only BL Lacs
$\log L_C/L_{\text{syn}}$	$\log L_{\text{inj}}^{\text{obs}}$	51	0.45 ± 0.06	-20.52 ± 2.94	0.725	5.9×10^{-9}	All
		37	0.27 ± 0.08	-11.84 ± 3.90	0.499	1.7×10^{-3}	Only FSRQ
		14	0.28 ± 0.15	-13.00 ± 6.88	0.487	7.7×10^{-2}	Only BL Lacs
$\log L_C/L_{\text{syn}}$	$\log \nu_{\text{peak}}^{\text{obs}}$	51	-0.54 ± 0.14	14.57 ± 3.39	0.493	2.4×10^{-4}	All
		37	-0.15 ± 0.16	5.19 ± 4.09	0.156	3.5×10^{-1}	Only FSRQ
		14	-0.25 ± 0.21	6.62 ± 5.35	0.324	2.6×10^{-1}	Only BL Lacs
$\log L_C/L_{\text{syn}}$	$\log B$	51	-0.98 ± 0.11	0.10 ± 0.13	0.783	1.2×10^{-9}	All
		37	-0.74 ± 0.07	0.58 ± 0.09	0.864	1.5×10^{-11}	Only FSRQ
		14	-0.82 ± 0.20	-0.30 ± 0.19	0.761	1.6×10^{-3}	Only BL Lacs
$\log U_B$	$\log U_r$	51	1.21 ± 0.13	-0.64 ± 0.33	0.791	2.3×10^{-9}	All
		37	1.39 ± 0.08	-0.57 ± 0.19	0.945	6.3×10^{-11}	Only FSRQ
		14	1.22 ± 0.21	0.27 ± 0.57	0.857	9.0×10^{-5}	Only BL Lacs

Table 5. The input parameters for the EC model reproducing the average SEDs determined by Fossati et al. (1998) by dividing into radio luminosity (L_R) bins BL Lacs and FSRQ belonging to complete samples. (1) Radio luminosity bin; (2) region size in units of 10^{15} cm; (3), (4) compactnesses in injected particles and external radiation field; (5) maximum energy of the injected particles; (6) energy of the peak of the stationary electron distribution; (7) spectral index of the injected particles; (8) magnetic field intensity (in Gauss). In the fits the relativistic Doppler factor (column 9) has been fixed at the value $\delta=15$.

Log L_R (1)	$R/10^{15}$ (2)	ℓ_{inj} (3)	ℓ_{ext} (4)	γ_{max} (5)	γ_{peak} (6)	s (7)	B (8)	δ (9)
41.5	10	7e-4	1e-5	1.0e6	2.5e4	3.0	0.441	15
42.5	10	1e-3	1e-3	2.0e5	2.0e3	2.8	0.745	15
43.5	30	5e-3	2e-2	3.0e4	5.0e2	3.0	1.075	15
44.5	40	5e-2	0.1	1.5e4	3.5e2	2.5	1.178	15
45.5	50	5e-1	5.0	6.0e3	1.5e2	2.8	6.082	15

Table 6. Results of the principal component analysis. EV stands for eigenvector. The first row of the table lists the percentage of the correlation accounted for by the different eigenvectors.

Variable	EV ₁	EV ₂	EV ₃	EV ₄	EV ₅	EV ₆
%	44.55	27.08	13.17	9.0	3.52	2.66
δ	-0.2408	-0.5922	-0.3525	0.5140	0.1872	-0.4098
ℓ_{inj}	0.5608	0.0623	-0.0525	-0.3317	0.0915	-0.7486
ℓ_{ext}	0.5242	-0.1578	-0.3110	0.2645	-0.7031	0.1982
γ_{peak}	-0.2086	0.4119	-0.8594	-0.2063	0.0652	0.0376
U_B	0.5510	0.0746	-0.1082	0.3196	0.6654	0.3663
R	0.0748	-0.6673	-0.1611	-0.6412	0.1234	0.3111